Structural and compositional diversity of fibrillin microfibrils in human tissues

DOI:
10.1074/jbc.RA117.001483

Document Version
Accepted author manuscript

Structural and compositional diversity of fibrillin microfibrils in human tissues

Alexander Eckersley[1], Kieran T. Mellody[1], Suzanne Pilkington[2], Christopher E.M. Griffiths[2,5], Rachel E.B. Watson[2,5], Ronan O'Cualain[3], Clair Baldock[1,4], David Knight[3], Michael J. Sherratt[1*]

From the [1]Division of Cell Matrix Biology & Regenerative Medicine, [2]Division of Musculoskeletal & Dermatological Sciences, [3]School of Biological Sciences, [4]The Wellcome Trust Centre for Cell-Matrix Research, Faculty of Biology, Medicine and Health, The University of Manchester and [5]NIHR Manchester Biomedical Research Centre, Central Manchester University Hospitals NHS Foundation Trust, Manchester Academic Health Science Centre, Manchester, UK

Running Title: *Structural diversity in human tissue fibrillin microfibrils*

*To whom correspondence should be addressed: Michael J. Sherratt: 1.529 Stopford Building, The University of Manchester, Oxford Rd, Manchester, M13 9PT, UK; michael.sherratt@manchester.ac.uk; Tel. +44 (0)161 275 1439; Fax. +44 (0)161 275 5171.

Keywords: Fibrillin microfibril, collagen VI, extracellular matrix, skin, eye, fibroblast, proteomics, atomic force microscopy, AFM, protein structure

ABSTRACT

Elastic fibres comprising fibrillin microfibrils and elastin are present in many tissues, including the skin, lung, and arteries where they confer elasticity and resilience. Although fibrillin microfibrils play distinct and tissue-specific functional roles, it is unclear whether their ultrastructure and composition differ between elastin-rich (skin) and elastin-poor (ciliary body and zonule) organs or after in vitro synthesis by cultured cells. Here, we used atomic force microscopy, which revealed that the bead morphology of fibrillin microfibrils isolated from the human eye differs from those isolated from the skin. Using newly developed pre-MS preparation methods and LC-MS/MS, we detected tissue-specific regions of the fibrillin-1 primary structure that were differentially susceptible to proteolytic extraction. Comparing tissue- and culture-derived microfibrils, we found that dermis- and dermal fibroblast–derived fibrillin microfibrils differ in both bead morphology and periodicity and also exhibit regional differences in fibrillin-1 proteolytic susceptibility. In contrast, collagen VI microfibrils from the same dermal or fibroblast samples were invariant in ultrastructure (periodicity) and protease susceptibility. Finally, we observed that skin- and eye-derived microfibril suspensions were enriched in elastic fibre– and basement membrane–associated proteins, respectively. LC-MS/MS also identified proteins (such as calreticulin and protein disulphide isomerase) that are potentially fundamental to fibrillin microfibril biology, regardless of their tissue source. Fibrillin microfibrils synthesised in cell culture lacked some of these key proteins (MFAPs 2 and 4 and fibrillin-2). These results showcase the structural diversity of these key extracellular matrix assemblies, which may relate to their distinct roles in the tissues where they reside.

Extracellular matrices (ECM) are commonly comprised of a diverse array of assemblies which make key contributions to tissue mechanics and cell-mediated homeostasis. Some of these assemblies, such as the fibrillar collagens and the elastic fibres, are large, insoluble and supra-macromolecular. Some are markedly long-lived; laid down early in development where they persist and undergo a process of maturation (1) and subsequent age and disease related accumulation of damage (2, 3). During these processes, the ultrastructure of these assemblies can be tissue specific (1). Therefore, although these ECM assemblies are present in multiple tissues, they may exhibit distinct development-mediated ultrastructures which have evolved to fulfil their unique functionality.

Elastic fibres (comprised of fibrillin microfibrils and elastin (4)), are present in many tissues including skin (5), lungs (6), arteries (7) and ligaments (8) where they play a major role in conferring elasticity and resilience (4). The fibrillin microfibril, along with elastin, is a key component of the elastic fibre and adopts a bead-on-a-string appearance (9) when extracted and viewed with atomic force microscopy (AFM) and electron microscopy (EM). Additionally, these microfibrils exist also as stand-alone assemblies, forming candelabra-like structures (10) (see review (11)) in the papillary dermis. They also play a role in tissue homeostasis, sequestering and storing the latent forms of members of the TGF-β (12, 13) and BMP family (14). In eyes, fibrillin microfibrils play a very different architectural role to skin. They form the ciliary zonules: stand-alone suspensory ligaments which connect the lens capsule to the ciliary muscle (15). These zonules come under tensile stress as the ciliary muscle exerts a strain to deform the lens during accommodation. Although fibrillin microfibrils appear structurally and compositionally similar in mammalian tissues and cell culture systems, and retain a bead-like structure (and presence of the main component: fibrillin-1) throughout different tissues (9), little is known whether they have evolved to be distinct in each. Only two studies have shown that fibrillin microfibril ultrastructure is tissue- and developmentally-dependent: In 1997, we showed that inter-tissue differences in mass and periodicity (inter-bead distance) exist in microfibrils derived from bovine foetal aorta and skin (16). We also showed that fibrillin microfibrils undergo a process of post-translational maturation as their mass increased during foetus development. Lu *et al.* also reported similar differences in bead morphology between bovine adult aorta- and ciliary zonule-derived fibrillin microfibrils (17).

Since fibrillin microfibrils are present in a variety of tissues, the different roles they play may be reflected in the ultrastructure they adopt. These inter-tissue comparisons have never been made in human, or between fibrillin microfibrils sourced from ciliary body (CB) and skin, where they play very different architectural and mechanical roles. Additionally, the fibrillin microfibril's biomolecular composition has never been compared between tissues. Although their ultrastructure has been extensively studied using AFM (18–20) and EM (9, 18, 21), characterisation of the biomolecular composition through conventional biochemical approaches such as gel electrophoresis can be problematic due to their large size and insolubility. As a consequence, it is necessary to develop proteomic approaches to characterise fibrillin microfibril composition.

Recently, De Maria *et al.* performed whole tissue proteomics on dissected human and bovine ciliary zonules, and effectively characterised the zonular proteome (22). However, to date, only a single published proteomic study, performed by Cain *et al.* (23), attempted to characterise both the structure and composition of fibrillin microfibrils purified from human tissue. Through LC-MS/MS, Cain *et al*. achieved a 30% primary coverage of fibrillin-1 and identified several microfibril associated proteins such as microfibril associated protein (MFAP) 2. They demonstrated that MS-based proteomic approaches have the potential to identify the proteins involved in these supramolecular ECM assemblies. However, they observed that peptide generation from the core fibrillin-1 proteins, and their interacting proteins, was challenging due to their large size and high number of cross-links (24). Since this study took place, over ten years ago, advances have been made in mass spectrometer technology allowing greater resolving power with expanded functionalities (25). Coupled with improved sample preparation, we believe that these proteomic approaches can be enhanced further to allow effective inter-tissue comparisons of fibrillin microfibril composition and structure.

In this study, we optimised two effective methods of pre-MS sample preparation: elastase digestion and SMART digestion™, for the enhanced generation of fibrillin peptides and their microfibril-associated proteins. This led to their improved compositional analysis via LC-MS/MS, compared to Cain *et al.* 2006 (23). We go on to test differences between the ultrastructure (bead morphology and inter-bead periodicity) using AFM and biomolecular composition (fibrillin-1 structural, enzymatic susceptibly and associated protein presence) using mass spectrometry (MS) of fibrillin microfibrils isolated from human eye (CB), human skin and cultured human dermal fibroblasts (HDFs). Since collagen VI microfibrils co-purify with fibrillin microfibrils in skin- and

HDF-derived samples, we use them as a comparative control. We perform these analyses to test the following hypotheses:

1. Fibrillin microfibril ultrastructure and composition is tissue-dependent.
2. Culture-derived, newly synthesised fibrillin microfibril ultrastructure and composition is distinct from that of native, mature, tissue-sourced microfibrils.

Results and Discussion

Elastase digestion methods enhance fibrillin-1 peptide generation and, combined with SMART™ digestion methods, enhance the detection of microfibril-associated proteins

To improve the generation of peptides from core microfibril components, porcine elastase, a highly active and non-specific enzyme (which preferentially cleaves leucine, isoleucine, alanine, serine, valine and glycine) (26, 27) was used instead of conventional trypsin-based methodologies (see review (28)). For human CB-derived fibrillin microfibrils, this method, along with the use of a latest-generation mass spectrometer, led to an improved primary coverage (33%) and domain coverage (76%) of fibrillin-1, compared to that achieved by Cain *et al*. (23) (30% primary, 64% domain) (Fig 1A) and, for the first time, the identification of peptides from the C-terminal region of fibrillin-1 (orange arrow). A similar primary sequence and domain coverage was achieved when applied to human skin. Crucially, this improved coverage was achieved by the digestion and MS of single CB and skin samples whereas Cain *et al.* (23) reported a total primary sequence coverage of 30% from peptides identified in 13 separately prepared human, Gu-HCl and/or trypsin treated ciliary zonule samples.

In order to improve peptide generation from proteins which co-purify with the microfibril, SMART™ digestion was used. Collectively, the elastase and SMART™ digestion methods led to the successful identification of 13 known microfibril-associated proteins (Fig. 1B) from human CB. These include annexin V, annexin II, and MFAP2, identified by Cain *et al.* (23) in 2006.

Fibrillin microfibril bead morphology is tissue-dependent

The fibrillin microfibril is composed predominantly of fibrillin-1 (approximately 8 monomers per single bead and inter-bead repeat) with a total mass of ~2.5 MDa per repeat (9). The average periodicity and bead width has been approximated to 56 nm and 19 nm respectively (for detailed breakdown of microfibril dimensions see: (9)). Our data showed that fibrillin microfibrils derived from human eye (CB) had a significantly higher mean central bead height than those derived from human skin. (Fig 2Ai). Central bead height frequency distributions indicate that the majority of eye-derived fibrillin microfibrils had larger beads than skin-derived (Fig. 2Aii). Additionally, average axial height profiles showed that although eye-derived fibrillin microfibrils beads are significantly higher within a ~10nm radius of the centre, they were significantly lower at the shoulder region, ~20nm from the peak (Fig. 2Aiii, orange arrow) than skin-derived. These height differences in bead morphology are further exemplified in the contour heat map (Fig. 2Aiv) where eye-derived microfibrils appear to have a more pronounced bead with a lower shoulder region than skin. Between beads, however, there was no significant difference in the mean periodicity of fibrillin microfibrils derived from eye and skin (Fig. 2Bi, ii)

Many past studies exclusively use differences in periodicity to gauge ultrastructural differences in fibrillin microfibrils (19, 29–32) and other fibrillar components of the ECM (19, 33–35). However, not only does the majority of the fibrillin microfibril's mass rest within the bead, much of microfibril's functionality is thought to be mediated via the interaction between the bead and its associated proteins (36–38). Our data showed that eye-derived fibrillin microfibril beads differ in morphology in comparison to skin-derived, but periodicity did not. By omitting analysis of the microfibril bead, these studies may have missed some key ultrastructural changes linked to health and disease.

The ultrastructural variances seen between the beads of adult human eye- and skin-derived fibrillin microfibrils are similar to those we observed previously (16) where differences were detected in bead mass of microfibrils from bovine foetal skin and aorta. Lu *et al.* (17) also detected

differences in bead morphology, including the shoulder regions, from bovine adult ciliary zonule and aorta.

Fibrillin-1 derived from human eye and skin exhibit inter-tissue, regional differences in elastase susceptibility

To further compare and substantiate the ultrastructural differences seen between CB and skin fibrillin microfibrils, it was necessary to look at their biomolecular composition (fibrillin-1 structure and known microfibril associated protein presence). Previous studies have used differences to fibrillin-1's susceptibility to proteolysis to gauge abnormalities in fibrillin microfibril structure (39) and function (40, 41). It is possible that the fibrillin-1 structure may exhibit regional differences in proteolytic susceptibilities depending on its tissue of origin.

LC-MS/MS-detected peptide hit patterns (23) indicate several regions of human eye-derived fibrillin-1 (Fig. 3) with differing susceptibilities to elastase in comparison to skin-derived (green brackets). These regional differences indicate that, not only are fibrillin microfibrils ultrastructurally variable between tissues, their fibrillin-1 structural composition may also be as well. Collectively, it suggests that these supramolecular assembles may have evolved distinct ultrastructures and compositions in order to cope with their different architectural, mechanical and biochemical roles in their respective tissues of origin. It is possible that the presence of different cell types within each tissue may have contributed to these differences. Baldwin *et al*. showed that the epithelial-mesenchymal state of retinal pigment epithelial (RPE) cells influenced their ability to assemble fibrillin microfibrils (42). Although fibroblasts (mesenchymal cells) are thought to be responsible for microfibril deposition in skin (43) and in eye (44), it remains unknown whether epithelial cells contribute to fibrillin microfibril synthesis *in vivo* (45). It is also unclear whether populations of fibroblasts from different tissues exhibit differences in epithelial-mesenchymal states as shown in RPE cells (42). It is possible, therefore, that different cell types (or cells in different states) may synthesise fibrillin microfibrils with localised differences in structure.

So far, we have demonstrated fibrillin microfibril ultrastructure and fibrillin-1 regional susceptibility is tissue-dependent. These differences may also relate to microfibril post-translational maturation in development. To study this, we applied the same analysis to newly synthesised fibrillin microfibrils derived from cultured HDFs and compared it to skin fibrillin microfibrils, derived *ex vivo.*

Newly synthesised, HDF-derived fibrillin microfibrils exhibit marked differences in ultrastructure compared to skin-derived

On average, cultured HDF-derived, newly synthesised, fibrillin microfibrils had a significantly lower central bead height than human skin-derived (Fig. 4Ai). Additionally, central bead height frequency distributions indicate a sub-population of cultured HDF-derived fibrillin microfibrils with smaller beads than human skin-derived (Fig. 4Aii, orange arrow). Average axial height profiles indicate that, although skin fibrillin microfibril beads have a significantly larger central peak height than cultured HDF-derived microfibrils, the reverse is true on the slopes of the beads (opposite to the shoulder region) (Fig 4Aiii, purple arrow). This difference in bead morphology is further shown in the contour heat map (Fig. 4Aiv). Skin-derived beads have a higher peak with a more pronounced slope (except near the shoulder region) than HDF-derived beads. This indicates that beads of newly synthesised fibrillin microfibrils from cultured-HDFs have a different morphology those derived from human skin.

On average, cultured HDF-derived fibrillin microfibrils also exhibited a significantly higher periodicity in comparison to skin-derived fibrillin microfibrils (Fig. 4Bi). In addition, periodicity frequency distributions show a large population of cultured HDF-derived fibrillin microfibrils with significantly higher periodicities than skin-derived (Fig. 4Bii).

Similar differences in fibrillin microfibril bead morphology and periodicity have been previously reported in three cases. The first is between tissues where we showed that bovine foetal aorta fibrillin microfibrils had a higher bead mass and a lower periodicity than those derived from skin (16) and where Lu *et al.* (17) also reported that aorta-derived fibrillin microfibrils had differing bead morphologies and a higher periodicity compared to those from bovine zonules. The second is during developmental microfibril maturation

where we also showed that the gradual increase in foetal fibrillin microfibril bead mass and the gradual decrease in periodicity correlated with gestation time (16). The third is during photoageing where two studies highlighted the structural susceptibility of fibrillin microfibrils to UV irradiation. We showed that a low-dose UVB irradiation of both HDF- and human skin-derived fibrillin microfibrils directly led to the marked loss and re-distribution of their bead mass and a significant increase in their periodicity (20). Since then our group has also showed that physiological doses of both solar simulated radiation (SSR) (~5% UVB and ~95% UVA) and pure UVA led to a significant decrease in the periodicity of HDF-derived fibrillin microfibrils (19).

Although these fibrillin microfibril ultrastructural differences have been reported between tissues, during maturation and in photodamage, this study has identified them between microfibrils derived *in vitro,* from primary fibroblasts (natively found in human skin) and those derived *ex vivo*, directly from human skin. It is possible, therefore, that 1) the fibrillin microfibrils generated by HDFs are structurally immature in comparison to native microfibrils sourced from skin (either through lack of development or through the cell culture process) or that 2) the native skin-derived microfibrils have accumulated structural damage during ageing in comparison to those newly synthesised from HDFs. The ageing process would be more intrinsic than extrinsic (photoageing) since abdominal skin is relatively photoprotected compared to forearm skin used in previous photoageing studies (5). Since elastic fibre production is commonly thought to be fibroblast-driven (43), these changes may have profound implication for skin regenerative therapies, especially if they are linked to developmental maturation or ageing.

Fibrillin-1 derived from newly synthesised, HDF fibrillin microfibrils exhibited regional differences in elastase susceptibility compared to skin-derived.

LC-MS/MS-detected peptide hit patterns (23) indicate that several regions of human skin-derived fibrillin-1 (Fig. 5) with differing susceptibilities to elastase in comparison to HDF-derived (purple brackets). The observations that: 1) these regions of cultured HDF-derived fibrillin-1 have a different structurally susceptibility to elastase than skin-derived and that 2) HDF-derived fibrillin microfibrils have different ultrastructures compared to skin (Fig. 4), all support the possibility that either newly synthesised fibrillin microfibrils, derived from HDFs, are structurally immature compared to the more developmental (46), long-lived (2) microfibrils from skin or that the skin-derived fibrillin microfibrils are exhibiting signs of ageing in comparison to those newly synthesised from cells.

It is possible that these long-lived (2), skin-derived fibrillin microfibrils may have accumulated age-related damage through the formation of oxidative cross-links (47) (see review: (48)) induced by the long-term exposure to reactive oxygen species (ROS) in tissue and also via the accrual of advanced-glycation end products on fibrillin-1 (49) (see review: (50)) This process may have led to a differential susceptibility to enzyme digestion, and to an accrual of sugar on the surface of the bead, which would explain the variations in bead morphology.

HDF and skin-derived collagen VI microfibril structure is conserved compared to the fibrillin microfibril

Like the fibrillin microfibril, tissue collagen VI microfibrils are long-lived (51), supramolecular, beaded assemblies (52). Both microfibrillar species are highly abundant in connective tissue (53) and, as such, regularly co-purify (19, 53). This allowed us to a make a useful comparison between periodicity differences in collagen VI microfibrils and periodicity differences of fibrillin microfibrils in the same skin- and HDF-derived samples. However, because collagen VI microfibril beads are relatively small in comparison to fibrillin microfibril beads (19), unfortunately, AFM resolution was not good enough to assess differences in collagen VI bead morphology. Encouragingly though, the optimised elastase method generated sufficient collagen VI alpha-3 (COL6A3) peptides (Figure S1) to enable its regional susceptibility to elastase to also be compared to fibrillin-1. These comparisons allow us to differentiate whether the changes seen so far, between newly synthesised fibrillin microfibrils in culture and those derived in tissue, extrapolate to another predominating component of the ECM.

The periodicity and elastase susceptibility differences seen between HDF- and skin-derived fibrillin microfibrils (Fig. 4B) are a stark contrast to that in collagen VI microfibrils within the same samples (Fig. 6A). Newly synthesised, cultured HDF-derived collagen VI microfibril periodicity was not significantly different to that of skin collagen VI microfibrils, derived *ex vivo* (Fig. 6Ai). In addition, no distinctly different sub-populations of collagen VI microfibrils were seen when looking at periodicity frequency distributions of cultured HDF- and skin-derived collagen VI microfibrils (Fig. 6Aii). In fact, both distributions follow almost the same pattern, suggesting there is very little difference in the periodicity of collagen VI microfibrils from these two sources, unlike the fibrillin microfibril (Fig. 4B).

LC-MS/MS-detected peptide hit patterns, in response to elastase digestion of COL6A3 (Fig. 6B), were similar at the triple helix region (52), at the N1-N4 region and at the C1 domain of both skin- and HDF-derived samples. This is, again, in contrast to fibrillin-1 which did exhibit regional differences in response to elastase digestion (Fig. 5). However, domains N5, N6 and N8 yielded many more peptides from skin-derived COL6A3 than from cultured HDF-derived (Fig 6B). Alternative splicing of COLA3 has been previously shown both in mice and in humans (54) and isoforms of this COL6A3 lacking domains N5 and N7-N10 has previously been identified in human cell lines (54, 55). It is possible, therefore, that cultured HDFs are also synthesising collagen VI microfibrils which are lacking these domains which would explain the reduction in peptide hits seen from these regions in the HDF-derived preparations compared to skin.

Previously, we showed that collagen VI microfibril ultrastructure (periodicity) is resistant to both UVA and SSR whereas fibrillin microfibril ultrastructure is susceptible (19). Additionally Watson *et al.* (56) demonstrated that collagen VI microfibril distribution is unaffected in photoaged skin also in contrast to fibrillin microfibrils in elastic fibres which are markedly reduced in photoaged skin (5). Kielty *et al*. also reported that skin-derived collagen VI microfibril ultrastructure was indistinguishable at each stage bovine foetal development (57) unlike fibrillin microfibril ultrastructure which is (16). The observations made in this study, that newly synthesised, HDF-derived collagen VI microfibrils are structurally similar to the long-lived microfibrils derived from tissue, corroborates evidence that they are resistant to age-related damage accumulation and that their ultrastructure may not undergo the developmental process of maturation seen in other components of the ECM. These findings are divergent in comparison to the degradation seen in fibrillin microfibrils in ageing and to their maturation process (16) and accentuate the complexity of the fibrillin microfibril in tissue development and ageing.

Differences in the presence of co-purifying microfibril-associated proteins may provide insight into tissue functions of fibrillin microfibrils

So far, differences have been observed in both the ultrastructure of fibrillin microfibrils and their fibrillin-1 regional susceptibility to elastase, derived, *ex vivo*, from eye and skin and *in vitro* from cultured HDFs. The fibrillin microfibril's function is tied to the network it forms with a wide variety of proteins within the ECM (see references in Table 1). It is possible, therefore, that gauging the presence of these associated proteins may provide insight into the role they play within a specific tissue and into the underlying composition of the fibrillin microfibril.

Within the eye, skin and HDF microfibril purifications, a large variety of known fibrillin microfibril associated proteins (21, 30, 37, 46, 58–71) were identified using LC-MS/MS (Table 1). A large proportion of these associated proteins, were uniquely detected in either tissue. Four proteins key to elastic fibre biology were identified in skin. The elastic fibre component elastin (21); Elastin microfibril interface-located protein (EMILIN)-2, key to the microfibril's deposition onto elastic fibres (71); fibulin-1 (69), which exists as an interface between elastin and the fibrillin microfibril; and fibulin-2 (66), which co-localises with elastic fibres *in vivo* . This indicates that fibrillin microfibrils play a dominating role as an elastic fibre component in skin. Conversely, four basement membrane proteins were identified in eye-microfibril samples: perlecan, which was shown to connect fibrillin microfibrils directly to basal laminas, along with two laminins and nidogen-1 which bind to perlecan itself (65). This

indicates that fibrillin microfibrils play a major role in linking basement membranes within the CB epithelium of the eye.

The advantage of size-exclusion chromatography-purified microfibril proteomic analysis over whole tissue is that we can state with high confidence that the associated proteins identified must have been bound to the fibrillin microfibrils. Many of the proteins (fibrillin-2, MFAP2, MFAP5 and LTBP2) which directly co-purified with eye-derived microfibrils (Table 1) were the same as those found in the human zonule proteome published by De Maria *et al.* (22). Two of these proteins, metalloproteinase inhibitor 2 (TIMP3) and alpha-2 macroglobulin (A2M) were also identified in these suspensions (Table S1), however, they had no previously published interactions with fibrillin microfibrils. Since these proteins (TIMP3 in particular) were two of the most abundant protease inhibitors found in their whole zonule proteome, they could be newly identified associated proteins of the fibrillin microfibrils. However, some of De Maria *et al'*s most abundant glycoproteins (emilin-1 and hemicentin-1) identified in their zonule proteome did not co-purify with our eye-derived fibrillin microfibrils. It could be that these proteins do not associate with the microfibrils directly, or that the enzymatic extraction process and purification procedures stripped them from the microfibrils.

Many of the detected fibrillin microfibril-associated proteins were shared between tissues (Table 1). This may provide key insight into identifying the integral components, fundamental to fibrillin microfibril assembly and function, regardless of the tissue of origin. Fibrillin microfibril assembly begins with the secretion of the fibrillin-1 monomer from the cell (60, 72) where it is N- and C-terminally processed by furin. It is proposed that the fibrillin-1 monomers then dimerise in the extracellular space (60) and that these dimers then form the basic intermediates for further microfibril assembly. This process is thought to occur at the cell surface through the homotypic interaction between the N- and C-termini of fibrillin-1 dimers (24). Microfibril assembly is thought to be cell driven, as previous studies have shown that the deposition of fibrillin microfibrils by fibroblasts requires both fibronectin and the RGD-dependent α5β1 integrins (70). The molecular chaperone calreticulin and the disulphide bond-forming protein disulphide isomerase (PDI), (60) were identified in skin, eye and HDF microfibril samples. Ashworth *et al.* showed that both these intracellular proteins bind to fibrillin-1 thereby inhibiting their dimerisation and preventing their intracellular aggregation. They go on to propose that when the fibrillin-1 monomers are then secreted from the cell, the loss of these binding partners leads to their dimerisation in the extracellular space. The microfibrils tested in this study were purified via size-exclusion chromatography which separates structures of high molecular weight (MDa) from those of lower (kDa). This means the fractions used should be enriched with only mature, fibrillin and collagen VI microfibrils of varying lengths. Theoretically, immature forms of fibrillin-1, already bound to calreticulin and PDI, could have associated to these mature microfibrils. However, the N-terminus and C-terminus of immature fibrillins are cleaved by furin (at positions 44 and 1732 respectively) (73, 74) only after secretion from the cell (72) . In all samples tested, LC-MS/MS failed to detect any peptides corresponding to these cleaved propeptides. This suggests that immature fibrillin-1 was not detected in any of the samples tested. As such, it is possible that the intracellular proteins calreticulin and PDI were released from cells during the extraction process, where they then associated to the mature fibrillin microfibrils. Another explanation for the presence of PDI in the extracellular space is the recent evidence of its secretion from cells via an activation of αvβ3 integrin (75). In either case, the co-purification of calreticulin and PDI supports their proposed roles in microfibril assembly.

The microfibril associated proteins (MFAPs) 5, 2 and 4 were also identified in microfibril samples from both eye and skin tissues. Gibson *et al.* previously showed in bovine that MFAP5 (also known as MAGP-2) is localised in CB but not in the zonule (76), in contrast to MFAP2 (also known as MAGP-1), which was found in both. This fits with our identification, since the microfibrils used in this study were extracted from human CB. However, De Maria *et al.*, did detect MFAP5 both in high abundance in the human zonule and in less abundance in the bovine zonule (22). It is possible that either the CB was a contaminant within De Maria *et al*. zonular samples (like in this study, they also detect the basement membrane proteins

nidogen and laminin which can be attributed to the CB epithelium) or that perhaps there exists a genuine disparity between the composition of human and bovine ciliary zonules.

MFAPs4 and 5 are both instrumental to the proper formation and organisation of elastic fibres (61, 64) by interacting and co-localising with fibrillin-1, tropoelastin and the cross-linking enzyme desmosine as well as promoting tropoelastin self-assembly on top of fibrillin microfibrils. MFAP2 (also known as MAGP-1) binds strongly to fibrillin microfibrils (63, 77) and was found to interact directly with both TGF-β and BMP-7 (78). Disrupting this interaction in mice, leads to a marked increase in TGF-β signalling attributed to the loss of its sequestration into the fibrillin microfibril network (79). As such, MFAP2 plays a key role in modulating fibrillin-growth factor signalling. Fibrillin-2, a key component of maturing fibrillin microfibrils in developing elastic (80) and non-elastic (81) tissues, was also identified in microfibril preparations from both eye and skin. It is likely that these fibrillin microfibril-associated proteins were identified from both tissues because of the fundamental role they play fibrillin microfibril assembly and function.

Fibrillin-2 and MFAPs 2 and 4, which were identified in both eye- and skin-derived microfibril samples, were not detected in cultured HDF-derived microfibril samples. The observation that all three HDF-derived fibrillin microfibril purifications lacked detection of fibrillin-2, MFAP2 and MFAP4 compared to tissue-derived, indicates the possibility that these microfibrils may be immature and functionally impaired in 1) forming mature fibrillin microfibrils, 2) forming elastic fibres and 3) modulating growth factor signalling. The differences seen in the ultrastructure and presence of key associated proteins, observed in cell-derived fibrillin microfibrils compared to tissue-derived, could be due to the limitations of the cell culture model itself. Removing HDFs from their native, homeostatic environments could have contributed directly to the formation of immature and possibly defective fibrillin microfibrils. Many studies have exclusively used cell culture-derived microfibrils to elucidate their functional role in the ECM (63, 82, 83). The differences seen in this study demonstrates a problem with this approach as functional observations based on cell-derived fibrillin microfibrils may not necessarily reflect that seen in native tissue.

The distinct profiles seen between HDF- and skin-derived fibrillin microfibrils may have also contributed to the differences bead morphology. MFAP2, for instance, binds to the fibrillin microfibril bead directly (38). As a consequence, it is possible that the redistribution of HDF-derived microfibril bead height compared to skin-derived (Fig. 4Aiv) may be due to the loss of these associated proteins from the surface.

Conclusion

Building upon previous evidence (16, 17), this study has found that not only is fibrillin microfibril bead morphology tissue-source dependent, but fibrillin-1 regional proteolytic susceptibility is too. This study is first to show ultrastructural and compositional changes between human fibrillin microfibrils from elastin-rich (skin) and elastin-poor (ciliary body) tissues, which have evolved to play very different architectural roles. Additionally, this study observed that newly synthesised fibrillin microfibrils derived from HDFs had a different bead morphology and periodicity compared to native skin-microfibrils. This indicated that these newly synthesised microfibrils may be structurally immature in comparison to those developmentally formed in tissue or that they may lack the structure-altering damage accumulation seen in microfibrils from aged tissue. Additionally, this study demonstrated that collagen VI microfibrils, derived from HDFs and skin, are relatively invariable in periodicity and in regional elastase susceptibility, in comparison to the fibrillin microfibril. Finally, this study found that analysing the presence of the fibrillin microfibril-associated proteins within skin, eye and HDF-derived samples provides insight into the role they play in the elastic fibre, and the basement membrane. Additionally, it allowed the potential identification of proteins which could be fundamental to fibrillin microfibril biology regardless of their tissue-source and the observation that newly-synthesised microfibrils from cell culture lacked some of these proteins.

Although the loss and deterioration of the fibrillin microfibril network in response to chronic photoageing has been observed immunohistochemically (5), the effects on fibrillin

microfibril ultrastructure, fibrillin-1 protease susceptibility and associated protein composition has yet to be studied. The techniques and methodology used in this tissue and culture comparison would be well suited to this goal.

Experimental Procedures

Study Design

Microfibrils were extracted and purified from adult human: 1) eye (ciliary body; CB) (N=3: M74 = male aged 74 years, F79, F76), 2) abdominal skin (N=3: F49, F55, F56) and 3) cultured human dermal fibroblasts (HDF) (N=3: M75, M76, M77). The ultrastructure of these purified fibrillin microfibrils (bead morphology and bead-bead periodicity), from these three different sources, was measured and compared using atomic force microscopy (AFM) (Fig. 7). The regional susceptibility of the fibrillin-1 domain structure to elastase digestion was measured and compared by counting the average number of LC-MS/MS detected PSMs from each domain. Finally, the presence of known microfibril-associated proteins was detected and compared for each of these purifications using LC-MS/MS.

Collagen VI microfibrils, which are also present in these purifications, were treated as a control and their periodicity, and COL6A3 regional susceptibility to elastase compared to that of the fibrillin microfibrils in the same samples.

Reagents and Human Tissue and Cell Acquisition

All chemicals were sourced from Sigma-Aldrich Co. Ltd (Poole, UK) unless stated otherwise. This study is conducted in accordance with the European Medicines Agency Note for Guidance on Good Clinical Practice and the Declaration of Helsinki 1964 (revised Seoul 2008). The use of human donor eye tissue was approved by the University of Manchester ethics committee (ethics ref#11305). Tissue was received within 24 hours of corneal dissection (for corneal transplant services) from the Manchester Eye Bank, in accordance with the Human Tissue Act. The CB was carefully dissected from each tissue sample followed by snap freezing in liquid nitrogen and storage at -80^{o}C.

Human abdominal skin samples were acquired from the University of Manchester Skin Health Biobank (MSHB). This biobank was approved by the North West 5 Research Committee (ref: 09/H1010/10). Samples were snap frozen in liquid nitrogen and stored at -80°C.

Primary human dermal fibroblasts were cultivated from skin biopsies taken from donor photoprotected buttock. The use of this skin was approved by North West Research Ethics Committee (ref# 14415) where all donors gave written and informed consent. All incubations and cultures were performed at 37^{o}C (5% CO_2). Biopsies were incubated in HBSS (Fisher Scientific, Loughborough, UK) with 10% dispase, overnight. The dermis was then dissected and minced prior to incubation in fibroblast media: DMEM (Fisher Scientific, Loughborough, UK) containing 10% foetal calf serum (FCS), 1% L-glutamine, 1% amphotericin and 1% penicillin-streptomycin (Pen-Strep; Gibco, Paisley, UK). Tissue samples were then cultured with weekly fibroblast media changes until HDFs could be observed on sample plates.

Microfibril Isolation and Purification

Human eye and skin tissue samples were minced and added to a 2ml aliquot of salt buffer (50mM Tris-HCl, 400mM NaCl and 1mM $CaCl_2$; pH 7.4). 1mg of bacterial collagenase IA, 0.01mM phenylmethylsulfonyl fluoride (PMSF) and 0.03 mM N-ethylmaleimide (NEM) was then added to the tissue which digested on a rotary mixer for 4 hours at room temperature (8, 19).

Post-confluent (passage 2) HDFs were maintained for 5 weeks in DMEM+GlutaMAX (Fisher Scientific, Loughborough, UK) containing 10% FCS and 50 μg/ml of Pen-Strep. HDFs were then washed with phosphate buffered saline (PBS) and 2ml of salt buffer was added directly to the culture flasks. 1mg of bacterial collagenase IA, 0.01mM PMSF and 0.03 mM NEM was then added and digested on an orbital shaker for 2 hours at room temperature.

Microfibril purification was achieved using an ÄKTA Prime Plus Liquid Chromatography System (GE Healthcare; Little Chalfont, UK). Post-digestion, tissue- and HDF-derived samples were centrifuged at 5000g for 5 min and supernatant was ran within a column buffer (comprised of 50mM Tris-HCl and 400mM NaCl at pH 7.4), through a GE HiScale 16/40 column containing Sepharose ® Cl2B beads (Sigma-Aldrich Co. Ltd), at 0.5ml/min. Co-purifying

fibrillin and collagen VI microfibrils were enriched in the void volume peak where fractions were collected based on spectrophotometric absorbance at 280nm (8, 19). Aliquots of the purification were kept for AFM, and rest were desalted in 0.22 µm filtered ultrapure water using a Slide-A-Lyzer™ MINI Dialysis Devices (Thermo Fisher Scientific; Paisley, UK) for 4 hours at 4°C. Samples were subsequently frozen at -80°C and freeze-dried at -60°C for 48 hours prior to storage at -80°C until their use in MS experiments.

Microfibril Peptide Generation using Elastase and SMART™ digestion prior to Mass Spectrometry

To enhance fibrillin-1 peptide generation, half of the freeze dried samples were re-suspended in 0.1M Tris-HCl, pH 8.5. Proteins were denatured in 8M urea, reduced in 10mM dithiothreitol (DTT) for 30 minutes at room temperature and alkylated using 50mM iodoacetamide (IAM) for 30 minutes at room temperature, in darkness. The solution was then diluted down to 2M urea, and elastase (Catalogue # E1250) added at a 2:1 enzyme to substrate ratio. This was incubated at 37°C for 4 hours. Elastase activity was then quenched with 5% formic acid in ultrapure water.

To enhance microfibril-associated protein peptide generation, the other half of the freeze-dried samples were re-suspended in ultrapure water and directly digested for 75 minutes using a SMART Digest™ kit (Thermo Scientific), which allows the fast digestion of the sample through immobilised trypsin beads, at a high, denaturing temperature (70°C) (84), as per the manufacturer's instructions. All samples were then desalted using POROS R3 (Life Technologies; Paisley, UK) beads and vacuum dried prior to MS analysis.

Mass Spectrometry

All MS was performed by the Biological Mass Spectrometry Core Facility in the Faculty of Biology, Medicine and Health at the University of Manchester (Manchester, UK). As dictated by their protocols (85, 86): vacuum dried samples were analysed by LC-MS/MS using an UltiMate® 3000 Rapid Separation LC (Dionex Corp; Sunnyvale, CA, USA) and an Orbitrap Elite mass spectrometer (Thermo Fisher Scientific). Peptide mixtures were separated using a gradient from 92% A (0.1% formic acid (FA) in water) and 8% B (0.1% FA in acetonitrile) to 33% B, in 30 min at 300nL min^{-1}, using a 250 mm x 75µm i.d. 1.7mM BEH C18, analytical column (Waters). Peptides were selected for fragmentation automatically by data dependent analysis.

Mass spectrometry data analysis

Mass spectra were extracted using extract_msn (Thermo Fisher Scientific) correlated against the Uniprot human database (87) using Mascot v2.5.1 (Matrix Science; London, UK).

Search parameters were: species - Homo sapiens; enzyme – trypsin for SMART™ Digested samples and non-specific for elastase digested samples; max missed cleavages – 1; fixed modifications - carbamidomethyl, mass – 57.02, AA – C; variable modification – oxidation, mass – 15.99, AA – M; peptide tolerance - 10 ppm (monoisotopic); fragment tolerance - 0.6 Da (monoisotopic); searched database: the SwissProt_2016_04 database (152,544 protein entries).

Data generated was validated using Scaffold (Proteome Software; Portland, OR, USA). Only exclusive, unique peptide counts are reported. False discovery rate (FDR) was calculated by Scaffold using protein and peptide probabilities assigned by the Trans-Proteomic Pipeline and the Protein Prophet™ (88) and Peptide Prophet™ (89) algorithm (Sourceforge; Seattle. WA, USA). Peptide Prophet FDR was thresholded to ≤5% and Protein Prophet FDR was thresholded to ≤0.1% (min 2 peptides) for every dataset.

The mass spectrometry proteomics data have been deposited to the ProteomeXchange Consortium via the PRIDE (90) partner repository with the dataset identifier PXD008450 and 10.6019/PXD008450.

Microfibril Atomic Force Microscopy

Glass coverslips were soaked in absolute ethanol overnight then attached to metal stubs with clear nail varnish. Samples were pipetted directly onto the coverslips and left for 1 minute so microfibrils could adsorb to the surface. Liquid was removed and stub left to dry overnight. Stubs were washed three times with ultrapure water and left to dry before being scanned using AFM. Fibrillin and collagen VI microfibrils were imaged using peak force and Scan-Asyst® mode on a Multimode 8 atomic force microscope (Bruker; Billerica, MA, USA), as previously described (18,19). Using a

single, new Scan-Asyst® Air tip (Bruker), single fibrillin MFs were captured at 512pixels/line in 2x2µm scans. This gave a resolution of 3.9nm/pixel, which was deemed high enough for fibrillin microfibril ultrastructural analysis (18,19). Fibrillin MFs which were laterally associated with collagen VI microfibrils were omitted from the analysis.

Scans were digitally flattened using WSxM v5.0 AFM Image Processing package (91) and exported in text image format. Height was corrected by subtracting negative background (92). Using ImageJ, fibrillin microfibrils were straightened using the Straighten Curved Objects plugin (93) enabling the generation of 41 pixel wide images of single straightened fibrillin microfibrils (Fig. 7). LFA image processing software, developed by our group using Microsoft Visual Basic 6.0 as previously described (94), was then used to specify the location of the maximum height of each bead and create a 15x41 pixel snapshot of each individual bead with the height maxima at the central pixel of the image. Maximum bead height and morphology were taken from these snapshots. Fibrillin microfibril periodicity was measured using Periodicity and Angles software package developed by our group using Microsoft Visual Basic 6.0 as previously described (95).

Acknowledgments: This study was funded by a programme Grant from Walgreens Boots Alliance, Nottingham, UK. The Wellcome Trust Centre for Cell-Matrix Research, University of Manchester is supported by core funding from the Wellcome Trust (088785/Z/09/Z). C.B and M.J.S acknowledge the support of the BBSRC (Ref: BB/N015398/1). The content is solely the responsibility of the authors and does not necessarily represent the official views of the National Institutes of Health.

Conflict of Interest: The authors declare that they have no conflicts of interest with the contents of this article. Walgreens Boots Alliance has approved this manuscript's submission but exerted no editorial control over the content.

Author Contributions: AE designed, performed all experiments, analysed all the data, prepared the figures and wrote the paper. MJS conceived and coordinated the study and contributed to the preparation of the figures and writing of the paper. SP contributed to the isolation of primary fibroblasts from human skin and KTM contributed to their cell culture. REBW and CEMG contributed to the study design and to the editing of the paper. DK and ROC provided technical assistance and support for all LC-MS/MS. CB contributed to the editing of the paper and interpretation of the results.

References

1. Parry, D. A. D., Barnes, G. R. G., and Craig, A. S. (1978) A comparison of the size distribution of collagen fibrils in connective tissues as a function of age and a possible relation between fibril size distribution and mechanical properties. *Proc. R. Soc. London B Biol. Sci.* **203**, 305–321
2. Shapiro, S. D., Endicott, S. K., Province, M. a., Pierce, J. a., and Campbell, E. J. (1991) Marked longevity of human lung parenchymal elastic fibers deduced from prevalence of D-aspartate and nuclear weapons-related radiocarbon. *J. Clin. Invest.* **87**, 1828–1834
3. Sell, D. R., and Monnier, V. M. (2010) Aging of Long-Lived Proteins: Extracellular Matrix (Collagens, Elastins, Proteoglycans) and Lens Crystallins. in *Comprehensive Physiology*, John Wiley {&} Sons, Inc., 10.1002/cphy.cp110110
4. Kielty, C. M., Sherratt, M. J., and Shuttleworth, C. A. (2002) Elastic fibres. *J. Cell Sci.* **115**, 2817–2828
5. Watson, R. E. B., Griffiths, C. E. M., Craven, N. M., Shuttleworth, C. A., and Kielty, C. M. (1999) Fibrillin-Rich Microfibrils are Reduced in Photoaged Skin. Distribution at the Dermal-Epidermal Junction. **112**, 782–787
6. Wright, R. R. (1961) Elastic Tissue of Normal and Emphysematous Lungs: A Tridimensional Histologic Study. *Am. J. Pathol.* **39**, 355–367
7. Wagenseil, J. E., and Mecham, R. P. (2009) Vascular extracellular matrix and arterial mechanics. *Physiol. Rev.* **89**, 957–989
8. Kielty, C. M., Cummings, C., Whittaker, S. P., Shuttleworth, C. a, and Grant, M. E. (1991) Isolation and ultrastructural analysis of microfibrillar structures from foetal bovine elastic tissues. Relative abundance and supramolecular architecture of type VI collagen assemblies and fibrillin. *J. Cell Sci.* **99 (Pt 4)**, 797–807
9. Baldock, C., Koster, A. J., Ziese, U., Rock, M. J., Sherratt, M. J., Kadler, K. E., Shuttleworth, C. A., and Kielty, C. M. (2001) The supramolecular organization of fibrillin-rich microfibrils. *J. Cell Biol.* **152**, 1045–1056
10. Cotta-Pereira, G., Rodrigo, G., and Bittencourt-Sampaio, S. (1976) Oxytalan, elaunin and elastic fibers in the human skin. *J Investig Dermatol.* **66**, 143–148
11. Naylor, E. C., Watson, R. E., and Sherratt, M. J. (2011) Molecular aspects of skin ageing. *Maturitas.* **69**, 249–256
12. Neptune, E. R., Frischmeyer, P. A., Arking, D. E., Myers, L., Bunton, T. E., Gayraud, B., Ramirez, F., Sakai, L. Y., and Dietz, H. C. (2003) Dysregulation of TGF-[beta] activation contributes to pathogenesis in Marfan syndrome. *Nat Genet*. **33**, 407–411
13. Kaartinen, V., and Warburton, D. (2003) Fibrillin controls TGF-β activation. *Nat. Genet.* **33**, 331–332
14. Sengle, G., Charbonneau, N. L., Ono, R. N., Sasaki, T., Alvarez, J., Keene, D. R., Bächinger, H. P., and Sakai, L. Y. (2008) Targeting of bone morphogenetic protein growth factor complexes to fibrillin. *J. Biol. Chem.* **283**, 13874–13888
15. Ashworth, J. L., Kielty, C. M., and McLeod, D. (2000) Fibrillin and the eye. *Br. J. Ophthalmol.* **84**, 1312–1317
16. Sherratt, M. J., Holmes, D. F., Shuttleworth, C. A., and Kielty, C. M. (1997) Scanning transmission electron microscopy mass analysis of fibrillin-containing microfibrils from foetal elastic tissues. *Int. J. Biochem. Cell Biol.* **29**, 1063–1070
17. Lu, Y., Sherratt, M. J., Wang, M. C., and Baldock, C. (2006) Tissue specific differences in fibrillin microfibrils analysed using single particle image analysis. *J Struct Biol*. **155**, 285–293
18. Sherratt, M. J., Baldock, C., Morgan, A., and Kielty, C. M. (2007) The morphology of adsorbed extracellular matrix assemblies is critically dependent on solution calcium concentration. *Matrix Biol.* **26**, 156–166
19. Hibbert, S. a., Watson, R. E. B., Gibbs, N. K., Costello, P., Baldock, C., Weiss, A. S., Griffiths, C. E. M., and Sherratt, M. J. (2015) A potential role for endogenous proteins as sacrificial sunscreens and antioxidants in human tissues. *Redox Biol.* **5**, 101–113

20. Sherratt, M. J., Bayley, C. P., Reilly, S. M., Gibbs, N. K., Griffiths, C. E., and Watson, R. E. (2010) Low-dose ultraviolet radiation selectively degrades chromophore-rich extracellular matrix components. *J Pathol*. **222**, 32–40
21. Sakai, L. Y., Keene, D. R., and Engvall, E. (1986) Fibrillin, a new 350-kD glycoprotein, is a component of extracellular microfibrils. *J. Cell Biol.* . **103**, 2499–2509
22. De Maria, A., Wilmarth, P. A., David, L. L., and Bassnett, S. (2017) Proteomic Analysis of the Bovine and Human Ciliary ZonuleProteomic Analysis of the Ciliary Zonule. *Invest. Ophthalmol. Vis. Sci.* **58**, 573–585
23. Cain, S. A., Morgan, A., Sherratt, M. J., Ball, S. G., Shuttleworth, C. A., and Kielty, C. M. (2006) Proteomic analysis of fibrillin-rich microfibrils. *Proteomics*. **6**, 111–122
24. Marson, A., Rock, M. J., Cain, S. A., Freeman, L. J., Morgan, A., Mellody, K., Shuttleworth, C. A., Baldock, C., and Kielty, C. M. (2005) Homotypic fibrillin-1 interactions in microfibril assembly. *J. Biol. Chem.* **280**, 5013–5021
25. Schilling, B., MacLean, B., Held, J. M., Sahu, A. K., Rardin, M. J., Sorensen, D. J., Peters, T., Wolfe, A. J., Hunter, C. L., and MacCoss, M. J. (2015) Multiplexed, scheduled, high-resolution parallel reaction monitoring on a full scan QqTOF instrument with integrated data-dependent and targeted mass spectrometric workflows. *Anal. Chem.* **87**, 10222–10229
26. Sziegoleit, a., Linder, D., Schluter, M., Ogawa, M., Nishibe, S., and Fujimoto, K. (1985) Studies on the specificity of the cholesterol-binding pancreatic proteinase and identification as human pancreatic elastase 1. *Eur. J. Biochem.* **151**, 595–599
27. Rietschel, B., Arrey, T. N., Meyer, B., Bornemann, S., Schuerken, M., Karas, M., and Poetsch, A. (2009) Elastase Digests: New Ammunition for Shotgun Membrane Proteomics. *Mol. Cell. Proteomics*. **8**, 1029–1043
28. Hustoft, H. K., Malerod, H., Wilson, S. R., Reubsaet, L., Lundanes, E., and Greibrokk, T. (2012) A critical review of trypsin digestion for LC-MS based proteomics. in *Integrative Proteomics*, InTech
29. Kielty, C. M., Davies, S. J., Phillips, J. E., Jones, C. J., Shuttleworth, C. A., and Charles, S. J. (1995) Marfan syndrome: fibrillin expression and microfibrillar abnormalities in a family with predominant ocular defects. *J. Med. Genet.* **32**, 1–6
30. Ashworth, J. L., Murphy, G., Rock, M. J., Sherratt, M. J., Shapiro, S. D., Shuttleworth, C. A., and Kielty, C. M. (1999) Fibrillin degradation by matrix metalloproteinases: implications for connective tissue remodelling. *Biochem J.* **340 Pt 1**, 171–181
31. Kielty, C. M., Raghunath, M., Siracusa, L. D., Sherratt, M. J., Peters, R., Shuttleworth, C. A., and Jimenez, S. A. (1998) The tight skin mouse: demonstration of mutant fibrillin-1 production and assembly into abnormal microfibrils. *J. Cell Biol.* **140**, 1159–1166
32. Hibbert, S. A., Costello, P., O'Connor, C., Bell, M., Griffiths, C. E. M., Watson, R. E. B., and Sherratt, M. J. (2017) A new in vitro assay to test UVR protection of dermal extracellular matrix components by a flat spectrum sunscreen. *J. Photochem. Photobiol. B Biol.* **175**, 58–64
33. Fang, M., Goldstein, E. L., Turner, A. S., Les, C. M., Orr, B. G., Fisher, G. J., Welch, K. B., Rothman, E. D., and Holl, M. M. B. (2012) Type I collagen D-spacing in fibril bundles of dermis, tendon and bone: bridging between nano-and micro-level tissue hierarchy. *ACS Nano*. **6**, 9503
34. Fang, M., Liroff, K. G., Turner, A. S., Les, C. M., Orr, B. G., and Holl, M. M. B. (2012) Estrogen depletion results in nanoscale morphology changes in dermal collagen. *J. Invest. Dermatol.* **132**, 1791–1797
35. Erickson, B., Fang, M., Wallace, J. M., Orr, B. G., Les, C. M., and Banaszak Holl, M. M. (2013) Nanoscale structure of type I collagen fibrils: quantitative measurement of D-spacing. *Biotechnol. J.* **8**, 117–126
36. Isogai, Z., Ono, R. N., Ushiro, S., Keene, D. R., Chen, Y., Mazzieri, R., Charbonneau, N. L., Reinhardt, D. P., Rifkin, D. B., and Sakai, L. Y. (2003) Latent transforming growth factor β-binding protein 1 interacts with fibrillin and is a microfibril-associated protein. *J. Biol. Chem.* **278**, 2750–2757

37. Isogai, Z., Aspberg, A., Keene, D. R., Ono, R. N., Reinhardt, D. P., and Sakai, L. Y. (2002) Versican interacts with fibrillin-1 and links extracellular microfibrils to other connective tissue networks. *J. Biol. Chem.* **277**, 4565–4572
38. Henderson, M., Polewski, R., Fanning, J. C., and Gibson, M. A. (1996) Microfibril-associated glycoprotein-1 (MAGP-1) is specifically located on the beads of the beaded-filament structure for fibrillin-containing microfibrils as visualized by the rotary shadowing technique. *J. Histochem. Cytochem.* **44**, 1389–1397
39. Gayraud, B., Keene, D. R., Sakai, L. Y., and Ramirez, F. (2000) New insights into the assembly of extracellular microfibrils from the analysis of the fibrillin 1 mutation in the tight skin mouse. *J. Cell Biol.* **150**, 667–680
40. Reinhardt, D. P., Ono, R. N., and Sakai, L. Y. (1997) Calcium stabilizes fibrillin-1 against proteolytic degradation. *J. Biol. Chem.* **272**, 1231–1236
41. Reinhardt, D. P., Ono, R. N., Notbohm, H., Müller, P. K., Bächinger, H. P., and Sakai, L. Y. (2000) Mutations in Calcium-binding Epidermal Growth Factor Modules Render Fibrillin-1 Susceptible to Proteolysis. *J. Biol. Chem.* **275**, 12339–12345
42. Baldwin, A. K., Cain, S. A., Lennon, R., Godwin, A., Merry, C. L. R., and Kielty, C. M. (2013) Epithelial-mesenchymal status influences how cells deposit fibrillin microfibrils. *J Cell Sci*
43. Long, J. L., and Tranquillo, R. T. (2003) Elastic fiber production in cardiovascular tissue-equivalents. *Matrix Biol.* **22**, 339–350
44. Stahnke, T., Löbler, M., Kastner, C., Stachs, O., Wree, A., Sternberg, K., Schmitz, K.-P., and Guthoff, R. (2012) Different fibroblast subpopulations of the eye: a therapeutic target to prevent postoperative fibrosis in glaucoma therapy. *Exp. Eye Res.* **100**, 88–97
45. Haynes, S. L., Shuttleworth, C. A., and Kielty, C. M. (1997) Keratinocytes express fibrillin and assemble microfibrils: implications for dermal matrix organization. *Br. J. Dermatol.* **137**, 17–23
46. Zhang, H., Apfelroth, S. D., Hu, W., Davis, E. C., Sanguineti, C., Bonadio, J., Mecham, R. P., and Ramirez, F. (1994) Structure and expression of fibrillin-2, a novel microfibrillar component preferentially located in elastic matrices. *J. Cell Biol.* **124**, 855–863
47. Wang, Z., Lyons, B., Truscott, R. J. W., and Schey, K. L. (2014) Human protein aging: modification and crosslinking through dehydroalanine and dehydrobutyrine intermediates. *Aging Cell*. **13**, 226–234
48. Stadtman, E. R. (1992) Protein oxidation and aging. *Science (80-.).* **257**, 1220–1224
49. Atanasova, M., Konova, E., Betova, T., and Baydanoff, S. (2009) Non-enzymatic glycation of human fibrillin-1. *Gerontology*. **55**, 73–81
50. Goldin, A., Beckman, J. A., Schmidt, A. M., and Creager, M. A. (2006) Advanced glycation end products. *Circulation*. **114**, 597–605
51. Sell, D. R., and Monnier, V. M. (2010) Aging of Long-Lived Proteins: Extracellular Matrix (Collagens, Elastins, Proteoglycans) and Lens Crystallins. in *Comprehensive Physiology*, John Wiley & Sons, Inc., 10.1002/cphy.cp110110
52. Baldock, C., Sherratt, M. J., Shuttleworth, C. A., and Kielty, C. M. (2003) The Supramolecular Organization of Collagen VI Microfibrils. *J. Mol. Biol.* **330**, 297–307
53. Kielty, C. M., Hanssen, E., and Shuttleworth, C. A. (1998) Purification of fibrillin-containing microfibrils and collagen VI microfibrils by density gradient centrifugation. *Anal. Biochem.* **255**, 108–112
54. Dziadek, M., Kazenwadel, J. S., Hendrey, J. A., Pan, T.-C., Zhang, R.-Z., and Chu, M.-L. (2002) Alternative splicing of transcripts for the alpha3 chain of mouse collagen VI: identification of an abundant isoform lacking domains N7–N10 in mouse and human. *Matrix Biol.* **21**, 227–241
55. Beecher, N., Roseman, A. M., Jowitt, T. A., Berry, R., Troilo, H., Kammerer, R. A., Shuttleworth, C. A., Kielty, C. M., and Baldock, C. (2011) Collagen VI, conformation of A-domain arrays and microfibril architecture. *J. Biol. Chem.* **286**, 40266–40275
56. Watson, R. E. B., Ball, S. G., Craven, N. M., Boorsma, J., East, C. L., Shuttleworth, C. A., Kielty, C. M., and Griffiths, C. E. M. (2001) Distribution and expression of type VI collagen in photoaged

skin. *Br. J. Dermatol.* **144**, 751–759
57. Kielty, C. M., Berry, L., Whittaker, S. P., Grant, M. E., and Shuttleworth, C. A. (1993) Microfibrillar assemblies of foetal bovine skin: developmental expression and relative abundance of type VI collagen and fibrillin. *Matrix*. **13**, 103–112
58. Cain, S. A., McGovern, A., Small, E., Ward, L. J., Baldock, C., Shuttleworth, A., and Kielty, C. M. (2009) Defining Elastic Fiber Interactions by Molecular Fishing: an affinity purification and mass spectrometry approach. *Mol. Cell. Proteomics*. **8**, 2715–2732
59. Meirelles, T., Araujo, T. L. S., Nolasco, P., Moretti, A. I. S., Guido, M. C., Debbas, V., Pereira, L. V, and Laurindo, F. R. (2016) Fibrillin-1 mgΔ lpn Marfan syndrome mutation associates with preserved proteostasis and bypass of a protein disulfide isomerase-dependent quality checkpoint. *Int. J. Biochem. Cell Biol.* **71**, 81–91
60. Ashworth, J. L., Kelly, V., Wilson, R., Shuttleworth, C. A., and Kielty, C. M. (1999) Fibrillin assembly: dimer formation mediated by amino-terminal sequences. *J. Cell Sci.* **112**, 3549–3558
61. Penner, A. S., Rock, M. J., Kielty, C. M., and Shipley, J. M. (2002) Microfibril-associated glycoprotein-2 interacts with fibrillin-1 and fibrillin-2 suggesting a role for MAGP-2 in elastic fiber assembly. *J. Biol. Chem.* **277**, 35044–35049
62. Dahlbäck, K., Ljungquist, A., Löfberg, H., Dahlbäck, B., Engvall, E., and Sakai, L. Y. (1990) Fibrillin immunoreactive fibers constitute a unique network in the human dermis: immunohistochemical comparison of the distributions of fibrillin, vitronectin, amyloid P component, and orcein stainable structures in normal skin and elastosis. *J. Invest. Dermatol.* **94**, 284–291
63. Trask, B. C., Trask, T. M., Broekelmann, T., and Mecham, R. P. (2000) The microfibrillar proteins MAGP-1 and fibrillin-1 form a ternary complex with the chondroitin sulfate proteoglycan decorin. *Mol. Biol. Cell*. **11**, 1499–1507
64. Pilecki, B., Holm, A. T., Schlosser, A., Moeller, J. B., Wohl, A. P., Zuk, A. V, Heumüller, S. E., Wallis, R., Moestrup, S. K., and Sengle, G. (2016) Characterization of Microfibrillar-associated Protein 4 (MFAP4) as a Tropoelastin-and Fibrillin-binding Protein Involved in Elastic Fiber Formation. *J. Biol. Chem.* **291**, 1103–1114
65. Tiedemann, K., Sasaki, T., Gustafsson, E., Göhring, W., Bätge, B., Notbohm, H., Timpl, R., Wedel, T., Schlötzer-Schrehardt, U., and Reinhardt, D. P. (2005) Microfibrils at basement membrane zones interact with perlecan via fibrillin-1. *J. Biol. Chem.* **280**, 11404–11412
66. Reinhardt, D. P., Sasaki, T., Dzamba, B. J., Keene, D. R., Chu, M.-L., Göhring, W., Timpl, R., and Sakai, L. Y. (1996) Fibrillin-1 and Fibulin-2 Interact and Are Colocalized in Some Tissues. *J. Biol. Chem.* **271**, 19489–19496
67. Ohno-Jinno, A., Isogai, Z., Yoneda, M., Kasai, K., Miyaishi, O., Inoue, Y., Kataoka, T., Zhao, J.-S., Li, H., and Takeyama, M. (2008) Versican and fibrillin-1 form a major hyaluronan-binding complex in the ciliary body. *Invest. Ophthalmol. Vis. Sci.* **49**, 2870–2877
68. Hirani, R., Hanssen, E., and Gibson, M. A. (2007) LTBP-2 specifically interacts with the amino-terminal region of fibrillin-1 and competes with LTBP-1 for binding to this microfibrillar protein. *Matrix Biol.* **26**, 213–223
69. Roark, E. F., Keene, D. R., Haudenschild, C. C., Godyna, S., Little, C. D., and Argraves, W. S. (1995) The association of human fibulin-1 with elastic fibers: an immunohistological, ultrastructural, and RNA study. *J. Histochem. Cytochem.* **43**, 401–411
70. Sabatier, L., Chen, D., Fagotto-Kaufmann, C., Hubmacher, D., McKee, M. D., Annis, D. S., Mosher, D. F., and Reinhardt, D. P. (2009) Fibrillin Assembly Requires Fibronectin. *Mol. Biol. Cell*. **20**, 846–858
71. Schiavinato, A., Keene, D. R., Wohl, A. P., Corallo, D., Colombatti, A., Wagener, R., Paulsson, M., Bonaldo, P., and Sengle, G. (2016) Targeting of EMILIN-1 and EMILIN-2 to fibrillin microfibrils facilitates their incorporation into the extracellular matrix. *J. Invest. Dermatol.* **136**, 1150–1160
72. Jensen, S. A., Aspinall, G., and Handford, P. A. (2014) C-terminal propeptide is required for

fibrillin-1 secretion and blocks premature assembly through linkage to domains cbEGF41-43. *Proc. Natl. Acad. Sci.* **111**, 10155–10160
73. Reinhardt, D. P., Gambee, J. E., Ono, R. N., Bächinger, H. P., and Sakai, L. Y. (2000) Initial Steps in Assembly of Microfibrils: Formation of disulfide-cross-linked multimers containing fibrillin-1. *J. Biol. Chem.* **275**, 2205–2210
74. Lönnqvist, L., Reinhardt, D., Sakai, L., and Peltonen, L. (1998) Evidence for furin-type activity-mediated C-terminal processing of profibrillin-1 and interference in the processing by certain mutations. *Hum. Mol. Genet.* **7**, 2039–2044
75. Ponamarczuk, H., Popielarski, M., Stasiak, M., Bednarek, R., Studzian, M., Pulaski, L., Babinska, A., and Swiatkowska, M. (2018) Contribution of activated beta3 integrin in the PDI release from endothelial cells. *Front. Biosci. (Landmark Ed.* **23**, 1612–1627
76. Gibson, M. A., Finnis, M. L., Kumaratilake, J. S., and Cleary, E. G. (1998) Microfibril-associated glycoprotein-2 (MAGP-2) is specifically associated with fibrillin-containing microfibrils but exhibits more restricted patterns of tissue localization and developmental expression than its structural relative MAGP-1. *J. Histochem. Cytochem.* **46**, 871–885
77. Gibson, M. A., Kumaratilake, J. S., and Cleary, E. G. (1989) The protein components of the 12-nanometer microfibrils of elastic and nonelastic tissues. *J. Biol. Chem.* **264**, 4590–4598
78. Weinbaum, J. S., Broekelmann, T. J., Pierce, R. A., Werneck, C. C., Segade, F., Craft, C. S., Knutsen, R. H., and Mecham, R. P. (2008) Deficiency in microfibril-associated glycoprotein-1 leads to complex phenotypes in multiple organ systems. *J. Biol. Chem.* **283**, 25533–25543
79. Walji, T. A., Turecamo, S. E., DeMarsilis, A. J., Sakai, L. Y., Mecham, R. P., and Craft, C. S. (2016) Characterization of metabolic health in mouse models of fibrillin-1 perturbation. *Matrix Biol.* **55**, 63–76
80. Mariencheck, M. C., Davis, E. C., Zhang, H., Ramirez, F., Rosenbloom, J., Gibson, M. A., Parks, W. C., and Mecham, R. P. (1995) Fibrillin-1 and fibrillin-2 show temporal and tissue-specific regulation of expression in developing elastic tissues. *Connect. Tissue Res.* **31**, 87–97
81. Yamanouchi, K., Tsuruga, E., Oka, K., Sawa, Y., and Ishikawa, H. (2012) Fibrillin-1 and fibrillin-2 are essential for formation of thick oxytalan fibers in human nonpigmented ciliary epithelial cells in vitro. *Connect. Tissue Res.* **53**, 14–20
82. Kielty, C. M., and Shuttleworth, C. A. (1993) The role of calcium in the organization of fibrillin microfibrils. *FEBS Lett.* **336**, 323–326
83. Kinsey, R., Williamson, M. R., Chaudhry, S., Mellody, K. T., McGovern, A., Takahashi, S., Shuttleworth, C. A., and Kielty, C. M. (2008) Fibrillin-1 microfibril deposition is dependent on fibronectin assembly. *J. Cell Sci.* **121**, 2696–2704
84. Moore, R., and Samonig, M. (2016) High-Throughput, High-Resolution Peptide Maps
85. Buckley, M. (2015) Ancient collagen reveals evolutionary history of the endemic South American " ungulates "
86. Lennon, R., Byron, A., Humphries, J. D., Randles, M. J., Carisey, A., Murphy, S., Knight, D., Brenchley, P. E., Zent, R., and Humphries, M. J. (2014) Global Analysis Reveals the Complexity of the Human Glomerular Extracellular Matrix. *J. Am. Soc. Nephrol.* 10.1681/ASN.2013030233
87. Consortium, U. (2014) UniProt: a hub for protein information. *Nucleic Acids Res.*
88. Nesvizhskii, A. I., Keller, A., Kolker, E., and Aebersold, R. (2003) A statistical model for identifying proteins by tandem mass spectrometry. *Anal. Chem.* **75**, 4646–4658
89. Keller, A., Nesvizhskii, A. I., Kolker, E., and Aebersold, R. (2002) Empirical statistical model to estimate the accuracy of peptide identifications made by MS/MS and database search. *Anal. Chem.* **74**, 5383–5392
90. Vizcaíno, J. A., Csordas, A., del-Toro, N., Dianes, J. A., Griss, J., Lavidas, I., Mayer, G., Perez-Riverol, Y., Reisinger, F., and Ternent, T. (2016) 2016 update of the PRIDE database and its related tools. *Nucleic Acids Res.* **44**, D447–D456
91. Horcas, I., Fernández, R., Gómez-Rodríguez, J. M., Colchero, J., Gómez-Herrero, J., and Baro, a. M. (2007) WSXM: A software for scanning probe microscopy and a tool for nanotechnology. *Rev.*

Sci. Instrum. 10.1063/1.2432410
92. Ratcliff, G. C., and Erie, D. a. (2001) A novel single-molecule study to determine protein-protein association constants. *J. Am. Chem. Soc.* **123**, 5632–5635
93. Kocsis, E., Trus, B. L., Steer, C. J., Bisher, M. E., and Steven, a C. (1991) Image averaging of flexible fibrous macromolecules: the clathrin triskelion has an elastic proximal segment. *J. Struct. Biol.* **107**, 6–14
94. Sherratt, M. J., Baldock, C., Louise Haston, J., Holmes, D. F., Jones, C. J. P., Adrian Shuttleworth, C., Wess, T. J., and Kielty, C. M. (2003) Fibrillin Microfibrils are Stiff Reinforcing Fibres in Compliant Tissues. *J. Mol. Biol.* **332**, 183–193
95. Sherratt, M. J., Bax, D. V, Chaudhry, S. S., Hodson, N., Lu, J. R., Saravanapavan, P., and Kielty, C. M. (2005) Substrate chemistry influences the morphology and biological function of adsorbed extracellular matrix assemblies. *Biomaterials*. **26**, 7192–7206

		Microfibril-Associated Protein Presence		
	Published Interaction	Eye	Skin	HDF
Annexin A2	Cain et al. 2009 (58)	***	***	***
Annexin A5	Cain et al. 2009 (58)	***	***	***
Vimentin	Cain et al. 2009 (58)	***	***	***
Protein disulphide-isomerase	Meirelles et al. 2016 (59)	***	***	***
Calreticulin	Ashworth et al. 1999a (60)	***	***	***
MFAP5 (MAGP2)	Penner et al. 2002 (61)	**	***	***
βig-h3	Cain et al. 2009 (58)	*	***	***
Versican	Isogai et al. 2002 (37)	*	***	***
MMP14	Ashworth et al. 1999b (30)	*	**	***
Prelamin-A/C	Cain et al. 2009 (58)	*	*	**
Vitronectin	Dahlbäck et al. 1990 (62)	***	**	
MFAP2 (MAGP1)	Trask et al. 2000 (63)	**	**	
MFAP4	Pilecki et al. 2016 (64)	*	***	
Fibrillin-2	Zhang et al. 1994 (46)	*	**	
Laminin β2	Tiedemann et al. 2005 (65)	***		*
SERBP1	Cain et al. 2009 (58)	*		*
IGFBP7	Cain et al. 2009 (58)	*		*
Fibulin-2	Reinhardt et al. 1996 (66)		**	**
Laminin α5	Tiedemann et al. 2005 (65)	***		
Nidogen-1	Tiedemann et al. 2005 (65)	**		
Perlecan	Tiedemann et al. 2005 (65)	**		
Hyaluronan link protein 1	Ohno-Jinno et al. 2008 (67)	*		
LTBP2	Hirani et al. 2007 (68)	*		
Elastin	Sakai et al. 1986 (21)		*	
Fibulin-1	Roark et al. 1995 (69)		*	
EMILIN-2	Schiavinato et al. 2016 (71)		*	
Fibronectin 1	Sabatier et al. 2009 (70)			***
Thrombospondin 1	Cain et al. 2009 (58)			***
MMP2	Ashworth et al. 1999b (30)			**
MMP3	Ashworth et al. 1999b (30)			*
Decorin	Trask et al. 2000 (63)			*

Peptide hit score	
>15	***
6-14	**
2-5	*

Table 1. A list of published fibrillin microfibril-associated proteins identified in eye, skin and HDF microfibril samples. Proteins, detected using LC-MS/MS (Protein Prophet FDR≤0.1%), along with their peptide hit score (sum of N=3) are shown.

Figure Legends

Figure 1. Elastase and SMART™ methods led to the improved detection of fibrillin-1 and improved identification of microfibril-associated proteins compared previous published efforts. The ability of the elastase method to produce peptides of fibrillin-1 from a single human ciliary body (CB) sample (female age 67 – F67) and a single human skin sample (F55) is compared to the efforts made by Cain *et al*. 2006 (A). As done by Cain *et al*, (23) peptide spectrum matches (PSMs) (Peptide Prophet FDR≤5%) were counted for each respective fibrllin-1 domain and heat mapped. Our method led to a greater primary coverage and domain coverage from a single sample run than Cain *et al*, whose coverages were achieved from 13 separate sample runs. Peptides from the C-terminal region of fibrillin-1 were also successfully detected (orange arrow) which Cain *et al* failed to identify. The known fibrillin microfibril-interacting protein identified by Cain *et al*. 2006 (green) are compared with those identified by elastase and SMART™ methods (Protein Prophet FDR≤0.1%, Peptide Prophet FDR≤5%) (B). The elastase method (red) and SMART™ method (blue) were both performed on the same human CB microfibril extract (F73). The elastase method appears to enhance the detection of microfibril-associated proteins thought to be tightly bonded to the structure (ie. the MFAP family) whereas the SMART™ method appears to enhance the detection of weakly interacting proteins (ie. versican and hyaluronan proteins). Collectively, these methods led to an enhanced detection of known microfibril-associated proteins compared to Cain *et al*. 2006 (23).

Figure 2. Fibrillin microfibril ultrastructure is tissue-source dependant. Eye-derived fibrillin microfibril mean central bead height was significantly higher (6.94nm; n=100 repeats/sample, averaged per microfibril; n=300 repeats in pooled data) than skin-derived (6.51nm; p=0.0023, Mann-Whitney U) (A, i). Cumulative frequency distributions of central bead height (averaged per microfibril, n=21 pooled) indicate a large population of eye-derived fibrillin microfibrils with significantly larger beads (p=0.0423; Kolmogorov-Smirnov) than skin-derived (A, ii). Axial bead profiles show that, although skin-derived fibrillin microfibril beads are significantly smaller, within ~10nm of the bead peak, than eye-derived (A, iii; Bonferroni corrected multiple comparison test), they also have significantly higher slopes at the shoulder regions than eye-derived (orange arrow). This may suggest that skin-derived fibrillin microfibril beads have a different volume distribution than that of eye-derived. To visualise these differences in bead morphology, the whole AFM height maps of skin-derived fibrillin microfibril beads were averaged and subtracted from that of eye-derived. The resulting height differences are represented as a heat map overlaid with the average height contour of the eye-derived beads (A, iv). The significant differences seen in the axial profile panel (iii) were also added to the heat map (iv, stars). The biggest differences in bead morphology were around the central peak where eye-derived beads were higher than skin and at the shoulder region where skin were higher than eye. There was no significant difference in the mean periodicity (p=0.9737; Mann-Whitney U, n=500 repeats/sample, averaged per microfibril; n=1500 repeats in pooled data) (B, i) and in the cumulative frequency distributions of periodicities (p=0.8580; Kolmogorov-Smirnov, averaged per microfibril, n=67 pooled) (B, ii) between eye- and skin-derived fibrillin microfibrils.

Figure 3. Eye-derived fibrillin-1 exhibits different regional patterns of elastase susceptibility compared to skin-derived. LC-MS/MS-detected fibrillin-1 PSMs (Peptide Prophet FDR≤5%) were counted for each respective protein domain, per sample (N=3), averaged (normalised based total spectrum count), and subsequently heat mapped to their corresponding domain. Eye-derived fibrillin-1 yielded more peptides between epidermal growth factor-like domains (EGF) 38 and EGF43 than skin-derived (53 total from eye-derived versus 24 total from skin-derived) (green brackets). Eye-derived fibrillin-1 also yielded more peptides at EGF16 and EGF17 than skin-derived (15 vs. 2), however, it yielded less peptides between EGF11 and EGF14 (14 vs. 39).

Figure 4. Newly synthesised, HDF-derived fibrillin microfibril ultrastructure is significantly different than native skin-derived. HDF-derived fibrillin microfibrils had significantly lower central bead heights (6.02nm; n=100 repeats/sample, averaged per microfibril; n=300 repeats in pooled data) than skin derived- (6.51nm, p=0.0038, Mann-Whitney U) (A, i). Cumulative frequency distributions of central bead height were not significantly different (p=0.1938, Kolmogorov-Smirnov; averaged per microfibril, n=21 pooled), however, they indicate a sub-population of HDF-derived fibrillin microfibrils with smaller beads than skin-derived (A, ii; orange arrow). Axial bead profiles (A, iii) show that skin-derived fibrillin microfibril beads are significantly higher than HDF-derived beads close to the central peak and significantly lower than HDF-derived beads at the slope opposite to the shoulder region (purple arrow) (Bonferroni corrected multiple comparison test; n=300 repeats pooled, averaged per microfibril). These changes in bead morphology are reflected in the height difference contoured heat map (A, iv) (AFM height maps of HDF-derived fibrillin microfibril beads were averaged and subtracted from that of skin-derived and subsequently heat mapped; the contour height of the average skin bead was then overlaid). Skin beads were higher than HDF beads only near the central peaks whereas HDF beads had higher slopes around the peaks (except near the shoulder region). HDF-derived fibrillin microfibrils exhibited a significantly higher periodicity (56.5nm; n=500 repeats/sample, averaged per microfibril; n=1500 repeats in pooled data) compared to skin-derived (54.4nm; p=0.0004, Mann Whitney U) (B, i). Periodicity cumulative frequency distributions indicate a large population of HDF-derived fibrillin microfibril with significantly higher periodicities (B, ii) in comparison to skin-derived (p=0.0051; Kolmogorov-Smirnov, averaged per microfibril, n=67 pooled).

Figure 5. Fibrillin-1, derived from newly synthesised, HDF fibrillin microfibrils exhibits different regional patterns of elastase susceptibility compared to skin-derived. LC-MS/MS-detected fibrillin-1 PSMs (Peptide Prophet FDR≤5%) were counted for each respective protein domain, per sample (N=3), averaged (normalised based total spectrum count), and subsequently heat mapped to their corresponding domain. Skin-derived fibrillin-1 yielded less peptides from the last five domains at the C-terminal region: between EGF43 and EGF47 (6 vs. 29) than HDF-derived, however, skin-derived yielded more peptides between EGF11 and EGF14 (39 vs. 22) than HDF-derived (purple brackets).

Figure 6. HDF- and skin-derived collagen VI microfibril ultrastructure, and its susceptibility to elastase, is predominantly invariant. There was no significant difference in periodicity between HDF-derived (108.2nm; n=500 repeats/sample, averaged per repeat; n=1500 repeats in pooled data) and skin-derived (108.2nm; p=0.6310, Mann-Whitney U) collagen VI microfibrils (A, i). Additionally, there was no significant difference between periodicity cumulative frequency distributions of HDF- and skin-derived collagen VI microfibrils (p=0.2656, Kolmogorov-Smirnov) (A, ii). LC-MS/MS-detected collagen VI alpha-3 (COL6A3) peptide sequences (Peptide Prophet FDR≤5%) were counted for each respective protein domain, per sample (N=3), averaged (normalised based total spectrum count), and subsequently heat mapped to their corresponding domain (B). There were similar PSM-patterns between skin- and HDF-derived COL6A3 in all regions except at domain N5,N6, and N8 which yielded more peptides from skin-derived (39 total) than HDF-derived (4 total). This analysis could not be effectively performed on eye-derived samples, due to low abundance of collagen VI microfibrils.

Figure 7. Ultrastructural measurements of the fibrillin microfibril, performed with AFM. Fibrillin microfibrils adopt a beads-on-a-string appearance when viewed with AFM. The height maps generated were used to measure and compare the bead morphology and the periodicity (inter-bead distance) of eye (CB)-, skin- and HDF-derived fibrillin microfibrils.

Fig. 1

A

Source	Method	Primary Coverage	Domain Coverage	Fibrillin-1 Peptide Hit Heat Map
Cain *et al.* – 13 human CZ samples	Trypsin + Gu-HCl	30%	64%	
Single human CB sample - F67	Elastase	33%	76%	
Single human skin sample - F55	Elastase	37%	83%	

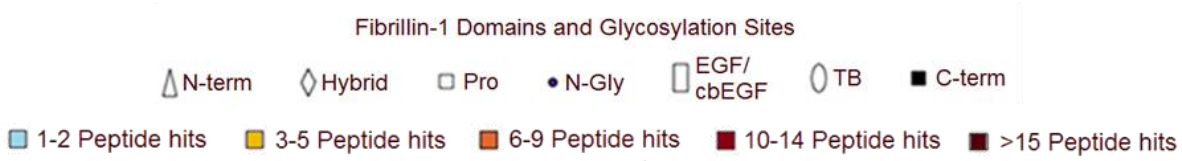

B

		Peptide Spectrum Matches	
Identified Associates	Cain *et al.* 2006 (3)	Elastase (10)	SMART™ (9)
Annexin V	✓	74	17
Annexin II	✓	52	17
MFAP2	✓	5	
Vimentin		11	18
Nidogen-1		2	5
Laminin β2		3	16
βig-H3		4	5
MFAP4		2	
MFAP5		7	
EMILIN-1		2	
Versican			3
Hyaluronan link-1			3
Prelamin-A/C			3

Fig. 2

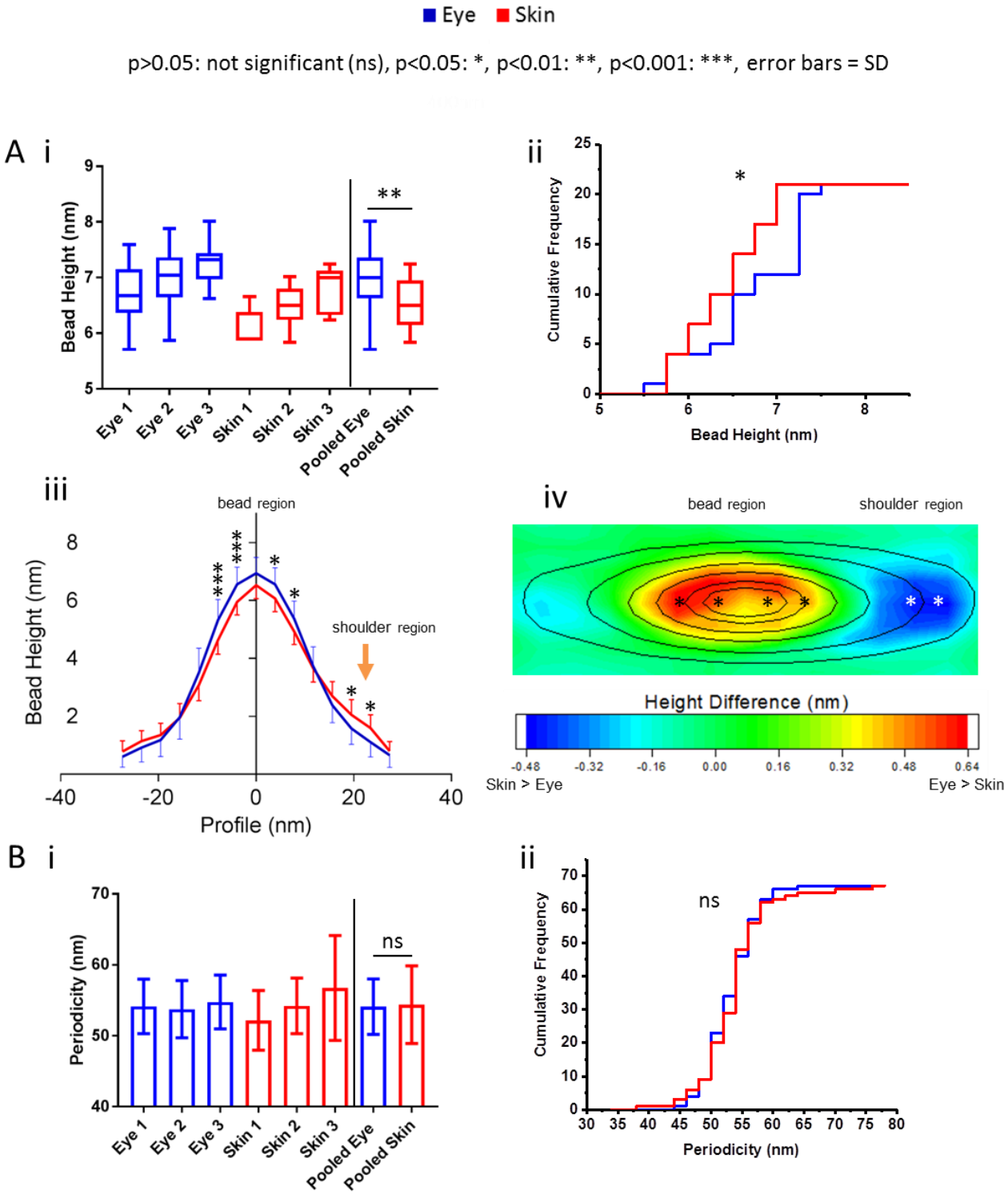
Eye
Skin
p>0.05: not significant (ns), p<0.05: *, p<0.01: **, p<0.001: ***, error bars = SD
A i
Bead Height (nm)
Eye 1
Eye 2
Eye 3
Skin 1
Skin 2
Skin 3
Pooled Eye
Pooled Skin
**
ii
Cumulative Frequency
Bead Height (nm)
*
iii
bead region
shoulder region
Bead Height (nm)
Profile (nm)
iv
bead region
shoulder region
Height Difference (nm)
-0.48
-0.32
-0.16
0.00
0.16
0.32
0.48
0.64
Skin > Eye
Eye > Skin
B i
Periodicity (nm)
ns
ii
Cumulative Frequency
Periodicity (nm)
ns

Fig. 3

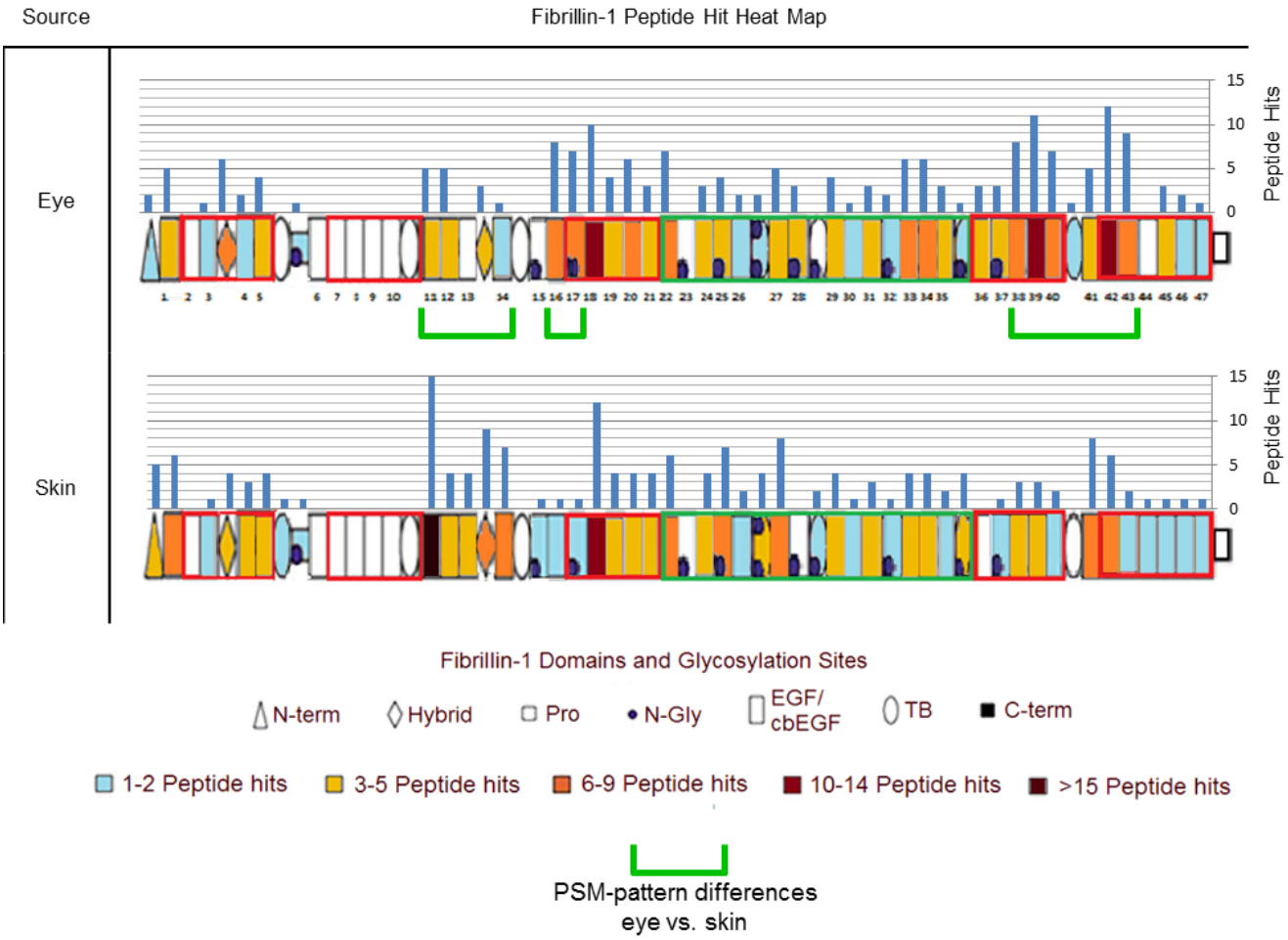
Source
Fibrillin-1 Peptide Hit Heat Map
Eye
Skin
Peptide Hits
15
10
5
0
Fibrillin-1 Domains and Glycosylation Sites
N-term
Hybrid
Pro
N-Gly
EGF/ cbEGF
TB
C-term
1-2 Peptide hits
3-5 Peptide hits
6-9 Peptide hits
10-14 Peptide hits
>15 Peptide hits
PSM-pattern differences eye vs. skin

Fig. 4

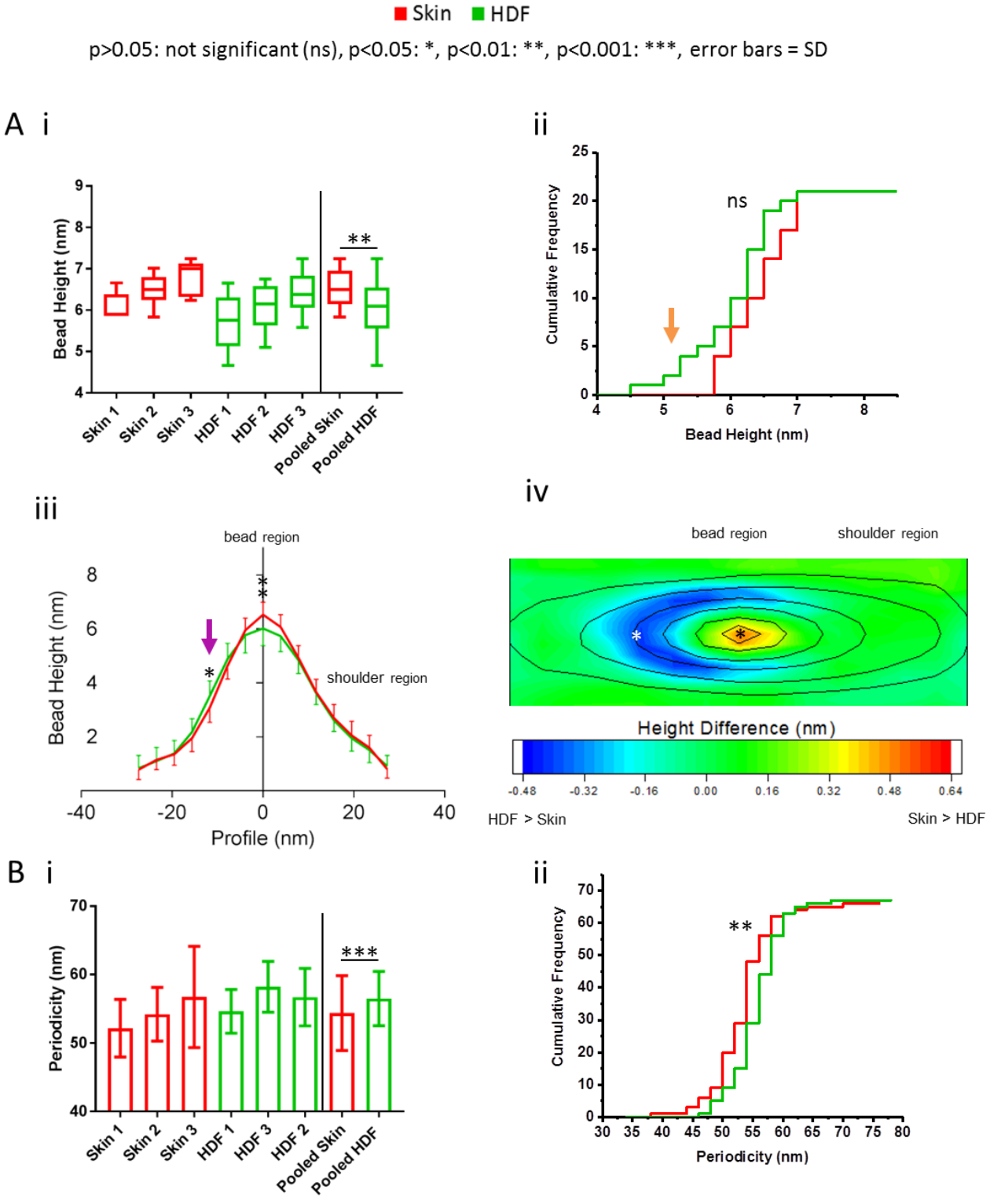
Skin HDF
p>0.05: not significant (ns), p<0.05: *, p<0.01: **, p<0.001: ***, error bars = SD
A i
Bead Height (nm)
Skin 1
Skin 2
Skin 3
HDF 1
HDF 2
HDF 3
Pooled Skin
Pooled HDF
**
ii
Cumulative Frequency
Bead Height (nm)
ns
iii
bead region
shoulder region
Bead Height (nm)
Profile (nm)
iv
bead region
shoulder region
Height Difference (nm)
HDF > Skin
Skin > HDF
B i
Periodicity (nm)
***
ii
Cumulative Frequency
Periodicity (nm)
**

Fig. 5

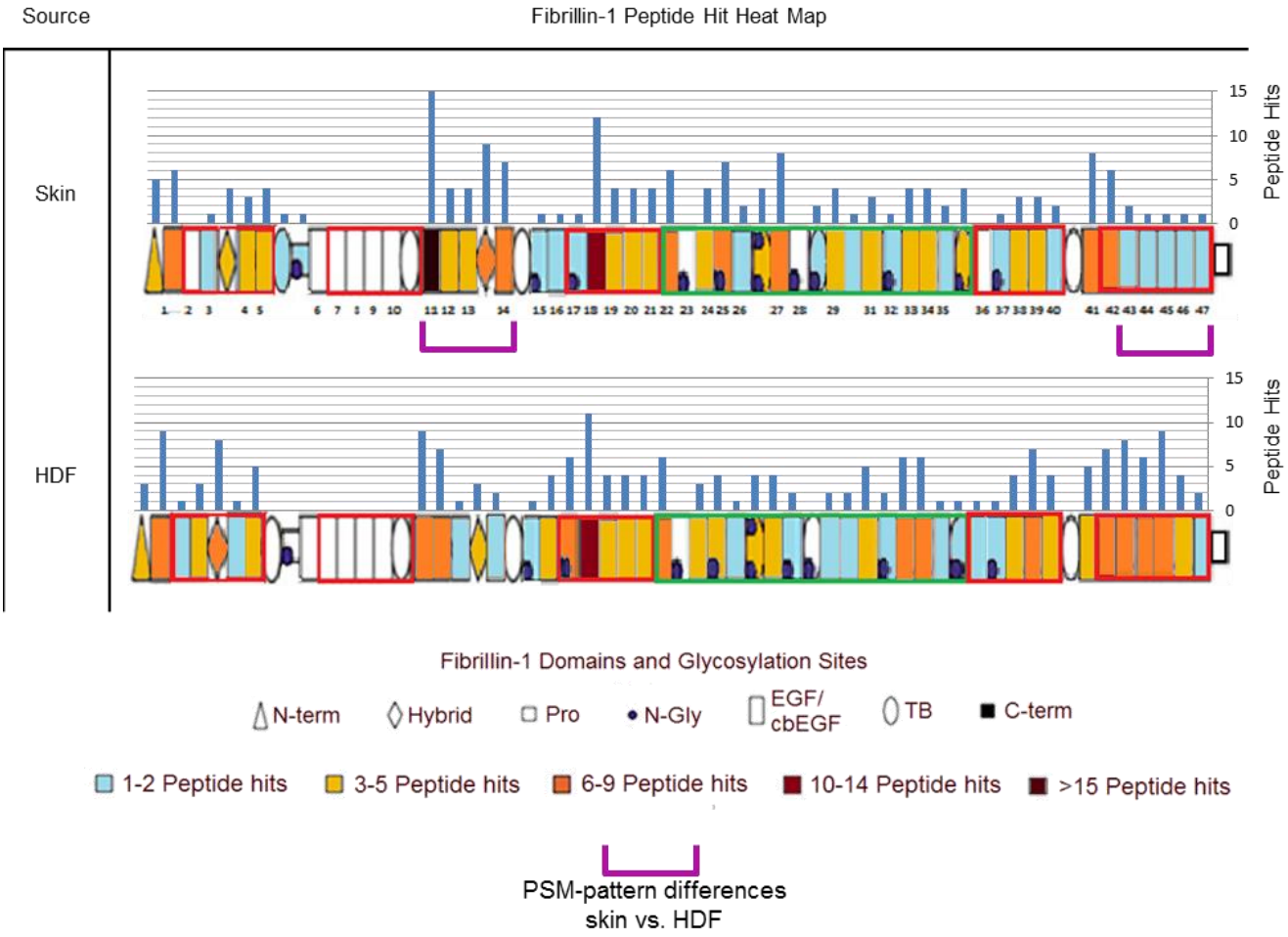
Source
Fibrillin-1 Peptide Hit Heat Map
Skin
HDF
Peptide Hits
15
10
5
0
Fibrillin-1 Domains and Glycosylation Sites
N-term
Hybrid
Pro
N-Gly
EGF/ cbEGF
TB
C-term
1-2 Peptide hits
3-5 Peptide hits
6-9 Peptide hits
10-14 Peptide hits
>15 Peptide hits
PSM-pattern differences skin vs. HDF

Fig. 6

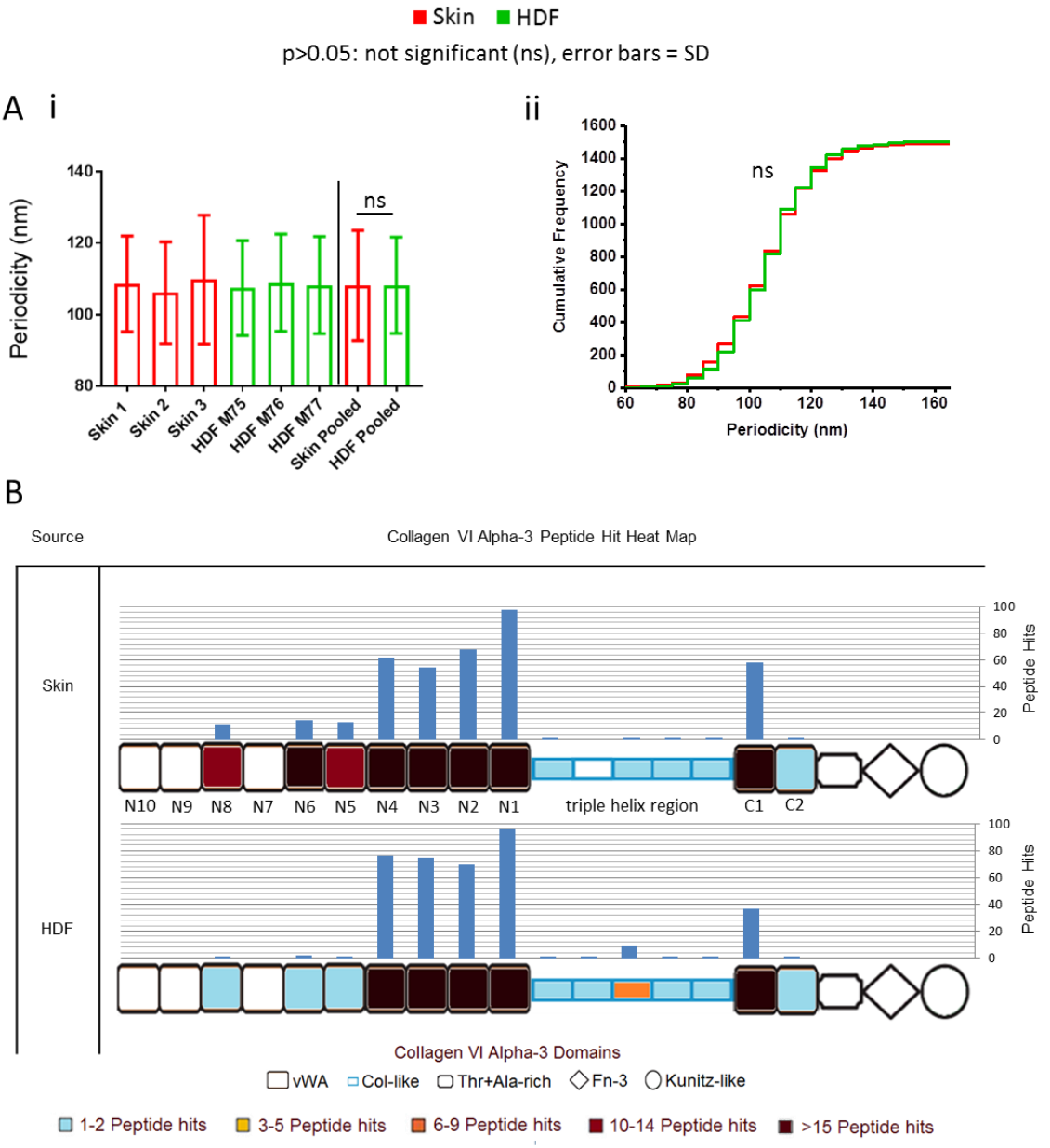
Skin
HDF
p>0.05: not significant (ns), error bars = SD
A i
Periodicity (nm)
140
120
100
80
ns
Skin 1
Skin 2
Skin 3
HDF M75
HDF M76
HDF M77
Skin Pooled
HDF Pooled
ii
Cumulative Frequency
1600
1400
1200
1000
800
600
400
200
0
ns
60
80
100
120
140
160
Periodicity (nm)
B
Source
Collagen VI Alpha-3 Peptide Hit Heat Map
Skin
HDF
Peptide Hits
100
80
60
40
20
0
N10
N9
N8
N7
N6
N5
N4
N3
N2
N1
triple helix region
C1
C2
Collagen VI Alpha-3 Domains
vWA
Col-like
Thr+Ala-rich
Fn-3
Kunitz-like
1-2 Peptide hits
3-5 Peptide hits
6-9 Peptide hits
10-14 Peptide hits
>15 Peptide hits

Fig. 7

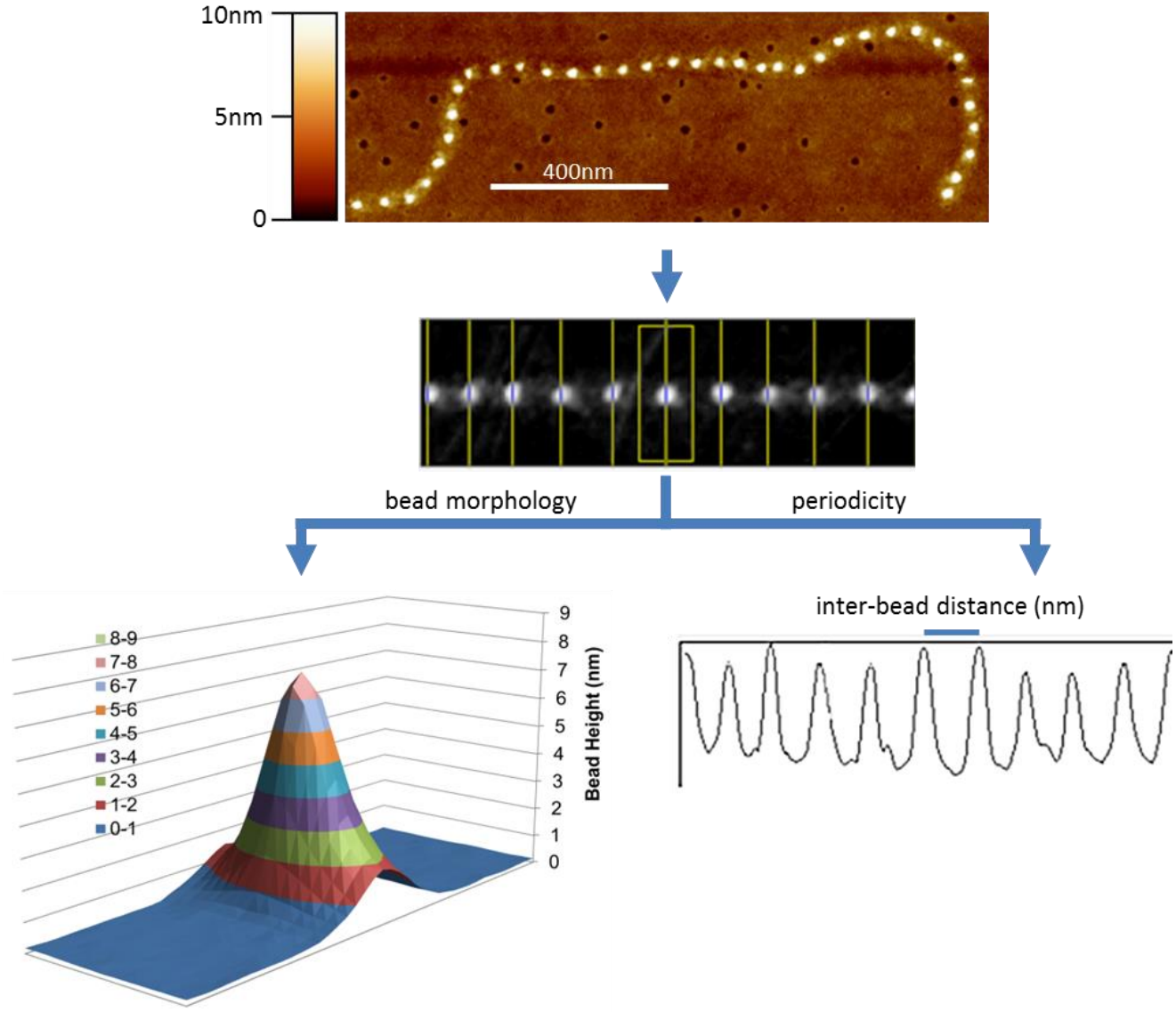
10nm
5nm
0
400nm
bead morphology
periodicity
8-9
7-8
6-7
5-6
4-5
3-4
2-3
1-2
0-1
Bead Height (nm)
9
8
7
6
5
4
3
2
1
0
inter-bead distance (nm)